Chapter 3
Mathematical Optimization of Unbalanced Networks with Smart Grid Devices

Carlos F. Sabillón, John F. Franco, Marcos J. Rider and Rubén Romero

Abstract Electric distribution networks should be prepared to provide an economic and reliable service to all customers, as well as to integrate technologies related to distributed generation, energy storage, and plug-in electric vehicles. A proper representation of the electric distribution network operation, taking into account smart grid technologies, is key to accomplish these goals. This chapter presents mathematical formulations for the steady-state operation of electric distribution networks, which consider the unbalance of three-phase grids. Mathematical models of the operation of smart grid related devices present in networks are discussed (e.g., volt-var control devices, energy storage systems, and plug-in electric vehicles). Furthermore, features related to the voltage dependency of loads, distributed generation, and voltage and thermal limits are also included. These formulations constitute a mathematical framework for optimization analysis of the network operation, which makes it possible to model decision-making processes. Different objectives related to technical and/or economic aspects can be pursued within the framework; in addition, the extension to multi-period and multi-scenario optimization is discussed. The presented models are built based on mixed integer linear programming formulations, avoiding the use of conventional mixed integer nonlinear formulations. The application of the presented framework

C. F. Sabillón (✉) · R. Romero
Department of Electrical Engineering, São Paulo State University (UNESP), Ilha Solteira, Brazil
e-mail: carlos.sabillon@unesp.br

R. Romero
e-mail: ruben.romero@unesp.br

J. F. Franco
São Paulo State University (UNESP), Rosana, Brazil
e-mail: j.f.franco@ieee.org

M. J. Rider
School of Electrical and Computer Engineering, University of Campinas, Campinas, Brazil
e-mail: mjrider@dsee.fee.unicamp.br

F. Shahnia et al. (eds.), *Electric Distribution Network Planning*, Power Systems, https://doi.org/10.1007/978-981-10-7056-3_3

is illustrated throughout control approaches for the voltage control and the plug-in electric vehicle charging coordination problems.

Keywords Distribution network operation · Mathematical optimization Mixed integer linear programming · Smart grids devices · Steady-state operation point

3.1 Introduction

At the present time, high levels of reliability are demanded to power systems, as electricity is required, among others, in industry, communication, lightning, heating and entertainment. Smart grids emerged from earlier attempts of power utilities to use the improvements on electronic technologies to bring a reliable supply of good quality electricity to their customers. Nowadays, smart grids stand out as the current responses in order to cope with the challenges brought by a rising electrical demand.

The electric distribution network is the final stage in the transfer of power to individual consumers. It routes power from small energy sources nearby or power substation fed by transmission lines, to residential, industrial, and commercial customers, through power lines, switches, and transformers [1]. Nowadays, utilities are in charge of operating the distribution network, maintaining a reliable supply of electric power to all costumers connected into the grid. Traditionally, the electrical distribution network has been designed to carry the power from the sources downstream to the consumers, but lately this one-way electricity delivery model has been changing.

With the evolution of the smart grids, the distributed generation (DG) growth, and the introduction of renewable sources and energy storage systems (ESS), the classic distribution network model is evolving. All of these factors impact directly over the planning, engineering, construction, operation, and maintenance of the network. As smart grids technologies continue to strengthen, the current electric distribution network will become a more intelligent and real-time optimized grid; in consequence, the complexity of the planning, operation, and maintenance of the network will increase, as new technologies and distribution practices, which offer greater efficiency, sustainability, and cost savings, are provided. Thereupon, the network must evolve in order to engage all network elements and participants including consumer, generators, and those that do both, in an active management seeking to fulfill technical, economic, and environmental objectives [2].

Since mid-1960s optimization concepts and techniques have been part of the power system planning and operation. The development of strong optimization methods and algorithms and their proper application to the power system depends on a suitable representation of the electric distribution network behavior under smart grid schemes. Hence, mathematical modeling is crucial to achieve an enhanced representation of the network operation, endorsing the decision-making of optimization algorithms.

Once a problem has been properly represented, it is up to the planners/operators to choose the most appropriate method in order to solve it. Heuristic and meta-heuristic techniques, as well as mathematical optimization have foregrounded among those techniques to become the most commonly applied methods to problem solving in electric distribution networks. In the latest years, the accelerated advent of efficient commercial solvers based on mathematical optimization has increased the interest of researchers in the development of complex and realistic mathematical models for optimization problems. Therefore, once the mathematical model is properly defined, the commercial solver finds the best solution; i.e., the planner/operator does not need to take care of the development of the solution method.

According to the nature of the adopted formulation for the optimization problem, the corresponding mathematical model may be classified as

- Linear Programming (LP), where the term 'linear' indicates that all constraints, as well as the objective function, are barren of any nonlinearity.
- Nonlinear Programming (NLP), which aims to deal with problems involving nonlinear constraints and/or objective function.
- Mixed Integer Linear Programming (MILP), which are a special type of LP, where all or some of the decision variables are confined to only integer values.
- Mixed Integer Nonlinear Programming (MINLP), a special type of NLP (analogue to MILP).

For each type of mathematical model there are several well-known optimization techniques. For example, LP problems can be solved by using simplex or interior point algorithms. For NLP problem one can use several traditional optimization techniques (gradient-based techniques, Lagrangian relaxation, Newton's method, successive linear programming, etc.) or an interior point algorithm. To solve MILP problems, a branch and bound algorithm, improved versions of branch and bound such as branch and price or branch and cut, Benders' decomposition, Gomory's cutting planes, among others, might be used. Finally, solving a MINLP problem is a very complicated task and there is few theory related to classical optimization in this regard. Thus, commercial solvers are assumed to solve this type of problems based on branch and bound algorithms, sensitivity and barrier methods, and interior point methods.

In the decade of 2000, commercial solvers based on classical optimization techniques excelled to become extremely efficient, taking advantage of the improvement on resolution techniques. Since then, solvers that target LP and MILP problems such as CPLEX [3], MOSEK [4], GUROBI [5], and similar, had become extremely efficient compared to prior versions. In counterpart, the development of specialized solvers on NLP and MINLP problems is still in progress.

Due to the aforementioned, the interest in the development of mathematical models to represent the operation and planning of electric distribution networks has grown among the researchers. Thereby, commercial solvers such as CPLEX have been used when the problem is represented by a LP or MILP mathematical model. On the other hand, for those cases in which the problems are represented by NLP or

MINLP formulations, these formulations have been transformed into equivalent or approximated LP problems, if possible, or have been solved using solvers for NLP or MINLP problems such as KNITRO [6] or BONMIN [7], even though NLP specialized software are not equally efficient (i.e., they cannot guarantee the global optimum of the problem and they usually demand high computational efforts).

In electric distribution networks, mathematical modeling has become an important tool, as it is widely used in operation and expansion planning problems, especially those including mixed integer programming. This is due to the fact that commonly planners and operators of electric distribution networks have to meet specific goals with limited sources. Hence, a great share of the optimization problems can be classified as 'yes' or 'no' problems, which may be represented by binary variables. Decisions such as

- schedule/not schedule, e.g., electric vehicle charging;
- build/not build, e.g., the construction of a new distribution line;
- K out of N, e.g., the number of capacitors operating in a bank; and
- N-possible values, e.g., the tap-position of a voltage regulator;

can be optimized using mathematical models [1].

Moreover, the inclusion of smart grid devices and technologies into the electric distribution network urge improvements in mathematical formulations previously employed to model the grid. The flexibility offered by smart grid devices demand higher levels of accuracy and resolution in the problem formulations, leading to more realistic but also more complex models. In this regard, the utilization of three-phase representation has become crucial in the solution of problems related to network operation. A three-phase representation, in despite of the commonly used single-phase, takes into account the imbalance in the network and allows the inclusion of mutual coupling effects, conveying to a more accurate determination of the steady-state operation point.

This chapter presents two mathematical formulations to represent the steady-state operation of unbalanced electric distribution networks. The network is initially represented by NLP models; hereupon, LP models are developed throughout linearization techniques and approximations, which are implemented in order to avoid the complexity associated with the solution of the NLP problems. These formulations constitute a framework that can be used by planners and operators as a tool inside optimization methods and algorithms aiming to optimize specific goals, guaranteeing by these means, the feasibility of the solutions found. Besides, constraints related to load conditions, DG features, and voltage and thermal limits are also included in both formulations.

3.2 Mathematical Representation of Unbalanced Electric Distribution Networks

Traditionally, the evaluation of the electric distribution network state has been determined by solving a power flow. The objective of the power flow is to determine, given a set of specific values, the steady-state operation point of the network, i.e., obtain the voltage magnitudes, phase angles in all nodes, and derived quantities (e.g., active and reactive power flows, current magnitudes in the circuits, and power loss). The power flow is a useful tool for the analysis of networks in steady-state, being widely utilized in real time operation, as well as in the planning of expansion and operation. This problem is typically modeled as a system of nonlinear equations, solved through iterative methods [8, 9].

In this section, two approaches are presented aiming to model the operation of an unbalanced electric distribution network. In contradistinction to the iterative trait proper of commonly used power flow methods, these formulations can be solved using mathematical optimization; and they can be extended in order to be used as tools in optimization analysis in order to mathematically formalize decision-making regarding different objectives related to technical and/or economic constraints. Thereupon, in order to determine the steady-state operation point of a network using mathematical optimization, the operation of the grid must be modeled as a conventional mathematical programming problem (3.1). These problems have as a common feature the involvement of optimization. A goal is established and defined as an objective function (f) which has to be maximized or minimized by the setting of a set of control variables (x) and subject to a set of constraints.

$$\begin{array}{ll} \max/\min & f(x) \\ \text{subject to:} & g(x) \leq 0; \\ & h(x) = 0; \end{array} \tag{3.1}$$

Although the behavior of an electric distribution network follows a set of nonlinear constraints, it is desired to reach LP representations, which avoid the complexity related to the solution of NLP problems. For this, the nonlinear set of equations is initially presented; later, linearization and approximation techniques are applied to reach an LP model, in each approach. Moreover, in this section all loads are considered as constant power loads.

3.2.1 Current-Based Mathematical Formulation

This formulation is based on the real and imaginary parts of currents through circuits and node voltages in the network. A single branch of an unbalanced network is depicted in Fig. 3.1 Each vector of voltages and currents represent the sum of the corresponding real and imaginary parts, e.g., $\overrightarrow{I} = I^{re} + jI^{im}$. Hence, the set of

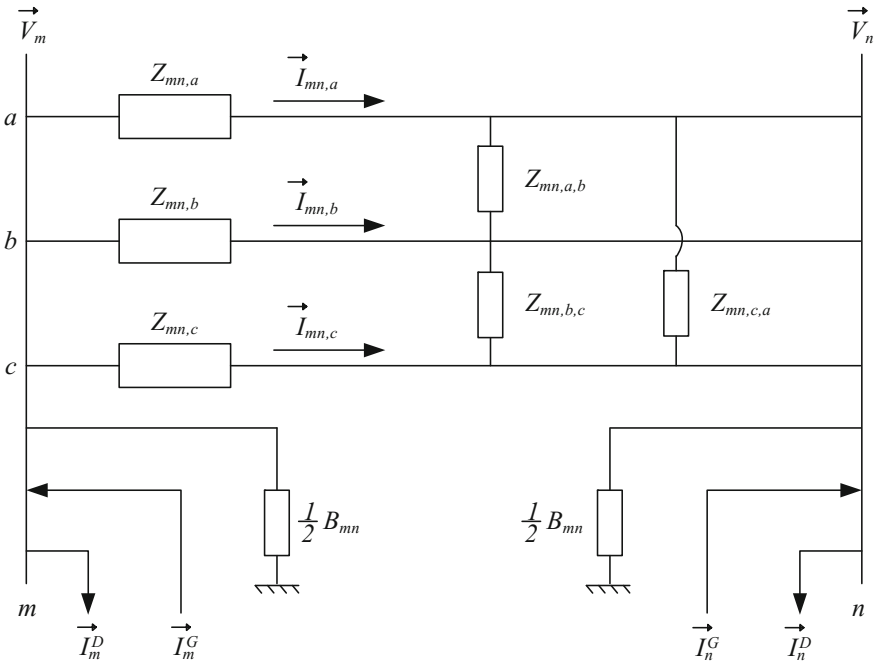

Fig. 3.1 Current-based representation of a single branch of an unbalanced electric distribution network

nonlinear mathematical relationships that represent the steady-state operation of an unbalanced network are written in terms of the current and voltages real and imaginary parts, the active and reactive power demanded by loads, and the circuit impedance, resistance, and reactance.

In the following formulation, consider the sets F, L, and N representing phases, circuits, and nodes, respectively. Furthermore, $V_{n,f}^{re/im}$ are the real/imaginary parts of the voltage at node n and phase f, while $I_{n,f}^{Gre/im}$ and $I_{n,f}^{Dre/im}$ are the real/imaginary parts of the generated and demanded currents, respectively. $P_{n,f}^{G/D}$ and $Q_{n,f}^{G/D}$ are the generated/demanded active and reactive powers. In addition, $I_{mn,f}^{re/im}$ represents the real/imaginary parts of the current through the circuit connecting nodes m and n, while $B_{mn,f}$ represents its shunt susceptance for phase f. Finally, $R_{mn,f,h}$ and $X_{mn,f,h}$ are the resistance and reactance for circuit mn between phases f and h, respectively.

From Fig. 3.1, the voltage drop from node m to node n can be derived as

$$\begin{bmatrix} \Delta\vec{V}_{mn,a} \\ \Delta\vec{V}_{mn,b} \\ \Delta\vec{V}_{mn,c} \end{bmatrix} = \begin{bmatrix} Z_{mn,a} & Z_{mn,a,b} & Z_{mn,a,c} \\ Z_{mn,a,b} & Z_{mn,b} & Z_{mn,b,c} \\ Z_{mn,a,c} & Z_{mn,b,c} & Z_{mn,c} \end{bmatrix} \begin{bmatrix} \vec{I}_{mn,a} \\ \vec{I}_{mn,b} \\ \vec{I}_{mn,c} \end{bmatrix} = \begin{bmatrix} Z_{mn,a}\vec{I}_{mn,a} + Z_{mn,a,b}\vec{I}_{mn,b} + Z_{mn,a,c}\vec{I}_{mn,c} \\ Z_{mn,a,b}\vec{I}_{mn,a} + Z_{mn,b}\vec{I}_{mn,b} + Z_{mn,b,c}\vec{I}_{mn,c} \\ Z_{mn,a,c}\vec{I}_{mn,a} + Z_{mn,b,c}\vec{I}_{mn,b} + Z_{mn,c}\vec{I}_{mn,c} \end{bmatrix} \tag{3.2}$$

Analyzing the individual case for phase a, (3.3) is formulated as

$$\Delta\vec{V}_{mn,a} = Z_{mn,a}\vec{I}_{mn,a} + Z_{mn,a,b}\vec{I}_{mn,b} + Z_{mn,a,c}\vec{I}_{mn,c} \tag{3.3}$$

Extending (3.3), considering that $Z_{mn,f,h} = R_{mn,f,h} + jX_{mn,f,h}$ and separating currents and voltages in their real and imaginary parts, (3.4) and (3.5) are obtained.

$$\begin{aligned} V^{re}_{m,a} - V^{re}_{n,a} = {} & R_{mn,a}I^{re}_{mn,a} + R_{mn,a,b}I^{re}_{mn,b} + R_{mn,a,c}I^{re}_{mn,c} - X_{mn,a}I^{im}_{mn,a} \\ & - X_{mn,a,b}I^{im}_{mn,b} - X_{mn,a,c}I^{im}_{mn,c} \end{aligned} \tag{3.4}$$

$$\begin{aligned} V^{im}_{m,a} - V^{im}_{n,a} = {} & R_{mn,a}I^{im}_{mn,a} + R_{mn,a,b}I^{im}_{mn,b} + R_{mn,a,c}I^{im}_{mn,c} + X_{mn,a}I^{re}_{mn,a} \\ & + X_{mn,a,b}I^{re}_{mn,b} + X_{mn,a,c}I^{re}_{mn,c} \end{aligned} \tag{3.5}$$

Generalizing these expressions, the voltage drop of an unbalanced network, written in terms of the real and imaginary parts of the voltages and currents, can be expressed by (3.6) and (3.7).

$$V^{re}_{m,f} - V^{re}_{n,f} = \sum_{h\in F}\left(R_{mn,f,h}I^{re}_{mn,h} - X_{mn,f,h}I^{im}_{mn,h}\right) \quad \forall mn \in L, f \in F \tag{3.6}$$

$$V^{im}_{m,f} - V^{im}_{n,f} = \sum_{h\in F}\left(X_{mn,f,h}I^{re}_{mn,h} + R_{mn,f,h}I^{im}_{mn,h}\right) \quad \forall mn \in L, f \in F \tag{3.7}$$

Furthermore, to model the complete steady-state operation of an unbalanced network, the first Kirchhoff's Law for the real and imaginary parts of the currents in each node is applied, as shown in (3.8) and (3.9). Hereupon, (3.10) and (3.11) establish the relationship between power, voltage and current for the loads.

$$\begin{aligned} & I^{Gre}_{m,f} + \sum_{km\in L} I^{re}_{km,f} - \sum_{mn\in L} I^{re}_{mn} - \left(\sum_{km\in L} B_{km,f} + \sum_{mn\in L} B_{mn,f}\right)\frac{V^{im}_{m,f}}{2} \\ & \quad = I^{Dre}_{m,f} \quad \forall m \in N, f \in F \end{aligned} \tag{3.8}$$

$$I_{m,f}^{Gim} + \sum_{km \in L} I_{km,f}^{im} - \sum_{mn \in L} I_{mn}^{im} - \left(\sum_{km \in L} B_{km,f} + \sum_{mn \in L} B_{mn,f} \right) \frac{V_{m,f}^{re}}{2} = I_{m,f}^{Dim} \quad \forall m \in N, f \in F \tag{3.9}$$

$$P_{n,f}^{D} = V_{n,f}^{re} I_{n,f}^{Dre} + V_{n,f}^{im} I_{n,f}^{Dim} \quad \forall n \in N, f \in F \tag{3.10}$$

$$Q_{n,f}^{D} = -V_{n,f}^{re} I_{n,f}^{Dim} + V_{n,f}^{im} I_{n,f}^{Dre} \quad \forall n \in N, f \in F \tag{3.11}$$

Equation (3.12) presents the complete NLP formulation developed to determine the steady-state operation point of an unbalanced network.

$$\begin{aligned} &\min \alpha \\ &\text{subject to : } (3.6) - (3.11) \end{aligned} \tag{3.12}$$

where α is the objective function of the NLP model, and can be designed to minimize or maximize the network operator best interests (e.g., power loss, voltage deviation, or reliability).

Aiming to achieve a LP model based on (3.12), linearization techniques and approximations must be applied to the nonlinearities shown in (3.10) and (3.11). In this regard, [10] proposed the application of Taylor's approximation around an estimated point $(V_{n,f}^{re^*}, V_{n,f}^{im^*})$. Hence, (3.10) and (3.11) are rewritten, expressing the real and imaginary currents in terms of the power and voltages, as shown in (3.13) and (3.14). Those equations represent the nonlinear expressions for the real and imaginary demanded currents as the functions $g(P_{n,f}^{D}, Q_{n,f}^{D}, V_{n,f}^{re}, V_{n,f}^{im})$ and $h(P_{n,f}^{D}, Q_{n,f}^{D}, V_{n,f}^{re}, V_{n,f}^{im})$, respectively.

$$I_{n,f}^{Dre} = \frac{P_{n,f}^{D} V_{n,f}^{re} + Q_{n,f}^{D} V_{n,f}^{im}}{V_{n,f}^{re2} + V_{n,f}^{im2}} = g(P_{n,f}^{D}, Q_{n,f}^{D}, V_{n,f}^{re}, V_{n,f}^{im}) \quad \forall n \in N, f \in F \tag{3.13}$$

$$I_{n,f}^{Dim} = \frac{P_{n,f}^{D} V_{n,f}^{im} - Q_{n,f}^{D} V_{n,f}^{re}}{V_{n,f}^{re2} + V_{n,f}^{im2}} = h(P_{n,f,t}^{D}, Q_{n,f,t}^{D}, V_{n,f,t}^{re}, V_{n,f,t}^{im}) \quad \forall n \in N, f \in F \tag{3.14}$$

Hereupon, taking advantage of the relatively small and limited variation range of the voltage magnitude in a distribution network, (3.15) and (3.16) present the Taylor's approximation used to linearize (3.10) and (3.11).

$$I_{n,f}^{Dre} = g^* + \frac{\partial g}{\partial V^{re}}\Big|^* (V_{n,f}^{re} - V_{n,f}^{re^*}) + \frac{\partial g}{\partial V^{im}}\Big|^* (V_{n,f}^{im} - V_{n,f}^{im^*}) \quad \forall n \in N, f \in F \tag{3.15}$$

$$I_{n,f}^{Dim} = h^* + \frac{\partial h}{\partial V^{re}}\Big|^* (V_{n,f}^{re} - V_{n,f}^{re^*}) + \frac{\partial h}{\partial V^{im}}\Big|^* (V_{n,f}^{im} - V_{n,f}^{im^*}) \quad \forall n \in N, f \in F \tag{3.16}$$

Therefore, the LP model that represents the steady-state operation of an unbalanced network is shown as

$$\begin{aligned} &\min \alpha \\ &\text{subject to}: (3.6)-(3.9), (3.15), \text{and } (3.16) \end{aligned} \tag{3.17}$$

3.2.2 Power-Based Mathematical Formulation

An additional representation to determine the steady-state operation point of an unbalanced network using mathematical optimization is presented. This formulation is based on the active and reactive power flow through the circuits and the voltage magnitudes in the network. Analogue to Figs. 3.1 and 3.2 shows a single branch of an unbalanced network, depicting the power flows through the circuits. Thus, each vector of complex power represents the sum of the active and reactive powers, i.e., $\overrightarrow{S} = P + jQ$.

For the following formulation let the sets F, L, and N, represent phases, circuits, and nodes, respectively. Besides, $\vec{V}_{n,f}$ is the voltage vector at node n and phase f, with magnitude $V_{n,f}$ and angle $\theta_{n,f}$; while, $V_{n,f}^{qdr}$ is the squared voltage magnitude at node n and phase f. Furthermore, $I_{mn,f}$ and $I_{mn,f}^{qdr}$ are the current magnitude and the squared current magnitude through circuit mn and phase f, respectively; while $P_{mn,f}$ and $Q_{mn,f}$ are the active and reactive power flows arriving at node n, respectively.

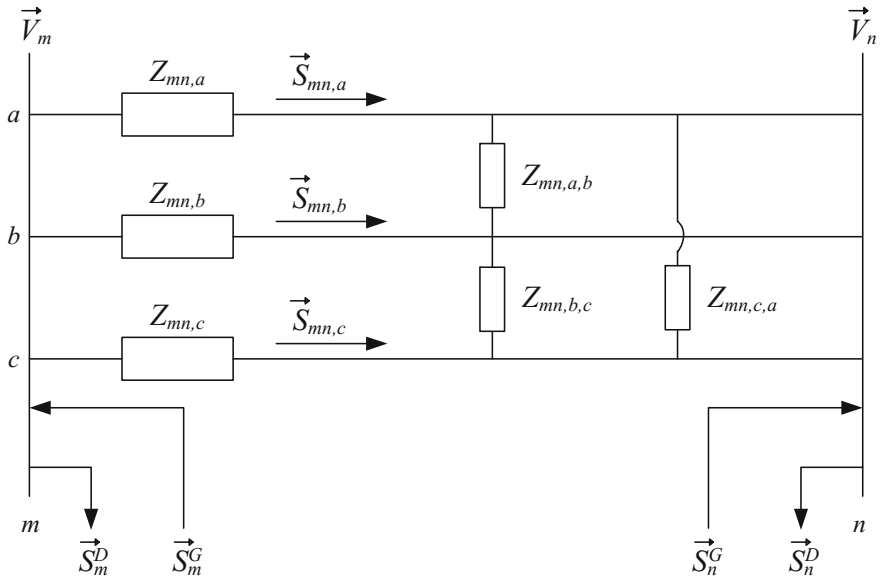

Fig. 3.2 Power-based representation of a single branch of an unbalanced electric distribution network

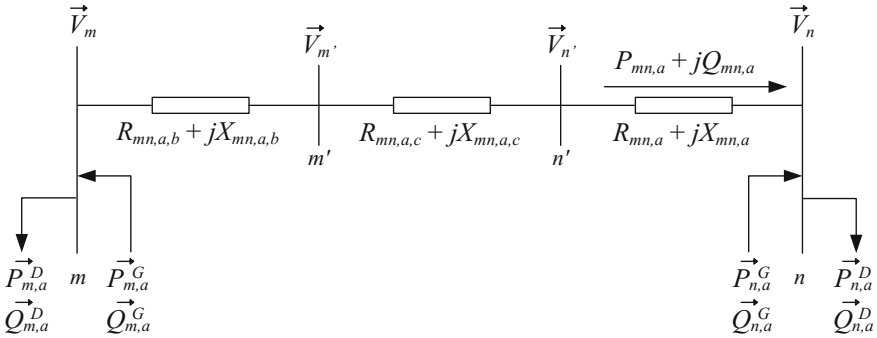

Fig. 3.3 Single branch equivalent for phase a

$S^{G/D}_{n,f}$, $P^{G/D}_{n,f}$ and $Q^{G/D}_{n,f}$ are the generated/demanded apparent, active, and reactive powers, respectively. Finally, $Z_{mn,f,h}, R_{mn,f,h}$, and $X_{mn,f,h}$ are the impedance, resistance, and reactance for circuit *mn* between phases *f* and *h*, respectively.

Hereby, $\vec{I}_{mn}$ in (3.2) must be expressed in terms of the active and reactive powers as shown in (3.18).

$$\vec{I}_{f,mn} = \left(\frac{\vec{S}_{f,mn}}{\vec{V}_{f,n}}\right)^* = \left(\frac{P_{f,mn} + jQ_{f,mn}}{\vec{V}_{f,n}}\right)^* \tag{3.18}$$

Analyzing only phase A from (3.2), Fig. 3.3 presents a simplified equivalent which divides the voltage drop considering two fictitious nodes m' and n'.

Therefore, the mathematical equations for each branch-segment are shown in (3.19).

$$\begin{aligned} \vec{V}_{m,a} - \vec{V}_{m',a} &= Z_{mn,a,b}\vec{I}_{mn,b} \\ \vec{V}_{m',a} - \vec{V}_{n',a} &= Z_{mn,a,c}\vec{I}_{mn,c} \\ \vec{V}_{n',a} - \vec{V}_{n',a} &= Z_{mn,a}\vec{I}_{mn,a} \end{aligned} \tag{3.19}$$

In order to reach a general expression for the voltage drop, each term of (3.19) is analysed separately. Initially, the first term can be written as shown in (3.20) where the term $\vec{V}^*_{m',a}/\vec{V}^*_{m',a}$ is added to enable some algebraic manipulations aiming to reach a approximated linear expression for the voltage drop.

$$\left(\vec{V}_{m,a} - \vec{V}_{m',a}\right) = \left(R_{mn,a,b} + jX_{mn,a,b}\right)\frac{P_{mn,b} - jQ_{mn,b}}{\vec{V}^*_{n,b}}\left(\frac{\vec{V}^*_{m',a}}{\vec{V}^*_{m',a}}\right) \tag{3.20}$$

Applying the simplification shown in (3.21), and replacing $(R_{mn,a,b}$ and $X_{mn,a,b})$ as presented in (3.22), constraint (3.23) is reached.

$$\frac{\vec{V}^{*}_{m',a}}{\vec{V}^{*}_{n,b}} \approx \frac{V_{m',a}}{V_{n,b}} \angle\left(\theta_{m,b} - \theta_{m,a}\right) \approx \frac{V_{m',a}}{V_{n,b}} \angle -120^{\circ} \tag{3.21}$$

$$\left(\tilde{R}_{mn,a,b} + j\tilde{X}_{mn,a,b}\right) = \left(R_{mn,a,b} + jX_{mn,a,b}\right)\left(1\angle -120^{\circ}\right) \tag{3.22}$$

$$\vec{V}_{m,a}\vec{V}^{*}_{m',a} - V^{2}_{m',a} = \frac{V_{m',a}}{V_{n,b}}\left(\tilde{R}_{mn,a,b} + j\tilde{X}_{mn,a,b}\right)\left(P_{mn,b} - jQ_{mn,b}\right) \tag{3.23}$$

By separating (3.23) into its real and imaginary parts, (3.24) and (3.25) are obtained.

$$V_{m,a}V_{m',a}\cos\left(\theta_{m,a} - \theta_{m',a}\right) = \frac{V_{m',a}}{V_{n,b}}\left(\tilde{R}_{mn,a,b}P_{mn,b} + \tilde{X}_{mn,a,b}Q_{mn,b}\right) + V^{2}_{m',a} \tag{3.24}$$

$$V_{m,a}V_{m',a}\sin\left(\theta_{m,a} - \theta_{m',a}\right) = \frac{V_{m',a}}{V_{n,b}}\left(\tilde{X}_{mn,a,b}P_{mn,b} - Q_{mn,b}\tilde{R}_{mn,a,b}\right) \tag{3.25}$$

Later, by adding the square power of (3.24) and (3.25), the expression for the voltage drop corresponding to the first segment of Fig. 3.3 is shown in (3.26).

$$V^{2}_{m,a} - V^{2}_{m',a} = 2\frac{V_{m',a}}{V_{n,b}}\left(\tilde{R}_{mn,a,b}P_{mn,b} + \tilde{X}_{mn,a,b}Q_{mn,b}\right) + \tilde{Z}^{2}_{mn.a.b}I^{2}_{mn,b} \tag{3.26}$$

Therefore, in order to avoid the nonlinearities shown in (3.26), assume $V_{m',a}/V_{n,a} \approx 1$, and the variables V^2 and I^2 are replaced by V^{sqr} and I^{sqr}, respectively. Hence,

$$V^{sqr}_{m,a} - V^{sqr}_{m',a} = 2\left(\tilde{R}_{mn,a,b}P_{mn,b} + \tilde{X}_{mn,a,b}Q_{mn,b}\right) + \tilde{Z}^{2}_{mn.a.b}I^{sqr}_{mn,b} \tag{3.27}$$

For the second term of (3.19), an analogue expression is obtained as shown in (3.27).

$$V^{sqr}_{m',a} - V^{sqr}_{n',a} = 2\left(\tilde{R}_{mn,a,c}P_{mn,c} + \tilde{X}_{mn,a,c}Q_{mn,c}\right) + \tilde{Z}^{2}_{mn.a.c}I^{sqr}_{mn,c} \tag{3.28}$$

Finally, for the last term of (3.19), the voltage drop is given by:

$$\left(\vec{V}_{n',a} - \vec{V}_{n,a}\right) = \left(R_{mn,a} + jX_{mn,a}\right)\frac{P_{mn,a} - jQ_{mn,a}}{\vec{V}^{*}_{n,a}} \tag{3.29}$$

For this segment it is considered that $R_{mn,a} + jX_{mn,a} = \tilde{R}_{mn,a} + j\tilde{X}_{mn,a}$, reaching the expression presented in (3.30).

$$V_{n',a}^{sqr} - V_{n,a}^{sqr} = 2\left(\tilde{R}_{mn,a}P_{mn,a} + \tilde{X}_{mn,a}Q_{mn,a}\right) + \tilde{Z}_{mn.a}^{2}I_{mn,a}^{sqr} \tag{3.30}$$

Therefore, the whole voltage drop in circuit *mn* is defined by (3.31), which considers coupling effects between the phases.

$$V_{m,f}^{sqr} - V_{n,f}^{sqr} = \sum_{h\in F}\left\{2 * \left(\tilde{R}_{mn,fh}P_{mn,f} + \tilde{X}_{mn,fh}Q_{mn,f}\right) + \tilde{Z}_{mn,fh}^{2}I_{mn,f}^{sqr}\right\} \quad \forall mn \in L, f \in F \tag{3.31}$$

In addition, the active and reactive power balances for each node are represented by (3.32) and (3.33), respectively. The calculation of the circuit current is given by (3.34).

$$\sum_{km\in L} P_{km,f} - \sum_{mn\in L}\left(P_{mn,f} + P_{mn,f}^{L}\right) + P_{m,f}^{G} = P_{m,f}^{D} \quad \forall m \in N, f \in F \tag{3.32}$$

$$\sum_{km\in L} Q_{km,f} - \sum_{mn\in L}\left(Q_{mn,f} + Q_{mn,f}^{L}\right) + Q_{m,f}^{G} = Q_{m,f}^{D} \quad \forall m \in N, f \in F \tag{3.33}$$

$$V_{n,f}^{sqr}I_{mn,f}^{sqr} = P_{mn,f}^{2} + Q_{mn,f}^{2} \quad \forall mn \in L, f \in F \tag{3.34}$$

To determine the power loss (P^L and Q^L), the complex power loss is initially expressed as

$$S_{mn,f}^{L} = \sum_{h\in\Omega_f} Z_{mn,f,h}\left(\frac{P_{mn,h} + jQ_{mn,h}}{\vec{V}_{m,h}}\right)^{*}\left(\frac{P_{mn,f} + jQ_{mn,f}}{\vec{V}_{m,f}}\right) \tag{3.35}$$

Equation (3.35) can be also written as

$$S_{mn,f}^{L} = \sum_{h\in\Omega_f} Z_{mn,f,h}\frac{\left(P_{mn,h} + jQ_{mn,h}\right)^{*}\left(P_{mn,f} + jQ_{mn,f}\right)}{\vec{V}_{m,f}\vec{V}_{m,h}\angle\left(\theta_{m,f} - \theta_{m,h}\right)} \tag{3.36}$$

Furthermore, replacing (3.22) in (3.36), it is obtained:

$$S_{mn,f}^{L} \approx \sum_{h\in\Omega_f} \tilde{Z}_{mn,f,h}\frac{\left(P_{mn,h} + jQ_{mn,h}\right)^{*}\left(P_{mn,f} + jQ_{mn,h}\right)}{\vec{V}_{n,f}\vec{V}_{n,h}} \tag{3.37}$$

Later, (3.37) and (3.38) are reached by separating the real and imaginary parts of (3.37). These constraints represent the power loss in an unbalanced network.

$$P^L_{mn,f} = \sum_{h\in\Omega_f} \tilde{R}_{mn,f,h} \frac{\left(P_{mn,f}P_{mn,h} + Q_{mn,f}Q_{mn,h}\right)}{V_{n,f}V_{n,h}} + \tilde{X}_{mn,f,h} \frac{\left(-Q_{mn,f}P_{mn,h} + P_{mn,f}Q_{mn,h}\right)}{V_{n,f}V_{n,h}} \quad \forall mn \in L, f \in F \tag{3.38}$$

$$Q^L_{mn,f} = \sum_{h\in\Omega_f} \tilde{X}_{mn,f,h} \frac{\left(P_{mn,f}P_{mn,h} + Q_{mn,f}Q_{mn,h}\right)}{V_{n,f}V_{n,h}} + \tilde{R}_{mn,f,h} \frac{\left(Q_{mn,f}P_{mn,h} - P_{mn,f}Q_{mn,h}\right)}{V_{n,f}V_{n,h}} \quad \forall mn \in L, f \in F \tag{3.39}$$

Finally, (3.40) represents the complete NLP model for the steady-state operation of an unbalanced network.

$$\begin{aligned} &\min \alpha \\ &\text{subject to } (3.31) - (3.34), (3.38), \text{ and } (3.39) \end{aligned} \tag{3.40}$$

The NLP model (3.40) contain nonlinearities [in constraints (3.34), (3.38), and (3.39)] that must be addressed to reach a LP model. Equation (3.34) has a product of two variables $\left(V^{sqr}_{n,f} \text{ and } I^{sqr}_{mn,f}\right)$ in the left-hand side and the square of two variables $\left(P_{mn,f} \text{ and } Q_{mn,f}\right)$ in the right-hand side. The left-hand side of (3.34) is linearized replacing the variable $V^{sqr}_{n,f}$ by an estimated value $\tilde{V}^2_{n,f}$. On the other hand, the right-hand side is approximated using a piecewise linearization technique (see Appendix 1). Hence, (3.41) shows the complete linear expression used to approximate (3.34).

$$\tilde{V}^2_{n,f} I^{sqr}_{mn,f} = f\left(P_{mn,f}, \overline{P_{mn,f}}, \Lambda\right) + f\left(Q_{mn,f}, \overline{Q_{mn,f}}, \Lambda\right) \quad \forall mn \in L, f \in F \tag{3.41}$$

Furthermore, as represented by (3.38) and (3.39), power loss can be approximated by any of the following options:

Option–A: Use actual, historic, or estimated values for the voltages and the power flows, in order to reach approximated values for P^L and Q^L in (3.32) and (3.33), disregarding (3.38) and (3.39), as shown in (3.42) and (3.43).

$$\sum_{km\in L} P_{km,f} - \sum_{mn\in L} \left(P_{mn,f} + \tilde{P}^L_{mn,f}\right) + P^G_{m,f} = P^D_{m,f} \quad \forall m \in N, f \in F \tag{3.42}$$

$$\sum_{km\in L} Q_{km,f} - \sum_{mn\in L} \left(Q_{mn,f} + \tilde{Q}^L_{mn,f}\right) + Q^G_{m,f} = Q^D_{m,f} \quad \forall m \in N, f \in F \tag{3.43}$$

In not fully observable distribution networks, a two-stage approach is recommended to estimate the power loss $\tilde{P}^{L}_{km,f}$ and $\tilde{Q}^{L}_{km,f}$. In the first stage, the LP is solved disregarding the power loss, i.e., $\tilde{P}^{L}_{km,f}$ and $\tilde{Q}^{L}_{km,f}$ are equal to zero. Later, the solution of stage one is used to initialize stage two and the LP model is once again solved.

If option A is chosen, the complete LP model will have the following form:

$$\begin{aligned} &\min \alpha \\ &\text{subject to } (3.31), \text{and } (3.41)-(3.43) \end{aligned} \tag{3.44}$$

Option–B: Use Taylor's approximation around an estimated point for the power flows and voltages $\left(P^{*}_{mn,f}, P^{*}_{mn,h}, V^{*}_{m,f} \text{and } V^{*}_{m,h}\right)$. Let the functions $g(P^{*}_{mn,f}, P^{*}_{mn,h}, Q^{*}_{mn,f}, Q^{*}_{mn,h}, V^{*}_{m,f}, V^{*}_{m,h})$ and $h(P^{*}_{mn,f}, P^{*}_{mn,h}, Q^{*}_{mn,f}, Q^{*}_{mn,h}, V^{*}_{m,f}, V^{*}_{m,h})$ be equal to the right part of (3.38) and (3.39), respectively. Equations (3.45) and (3.46) show the Taylor's approximation used to determine the power loss.

$$\begin{aligned} P^{L}_{mn,f} = g^{*} &+ \frac{\partial g}{\partial P_{mn,f}}\bigg|^{*}(P_{mn,f} - P^{*}_{mn,f}) + \frac{\partial g}{\partial P_{mn,h}}\bigg|^{*}(P_{mn,h} - P^{*}_{mn,h}) \\ &+ \frac{\partial g}{\partial Q_{mn,f}}\bigg|^{*}(Q_{mn,f} - Q^{*}_{mn,f}) + \frac{\partial g}{\partial Q_{mn,h}}\bigg|^{*}(Q_{mn,h} - Q^{*}_{mn,h} \quad \forall mn \in L, f \in F \\ &+ \frac{\partial g}{\partial V_{m,f}}\bigg|^{*}(V_{m,f} - V^{*}_{m,f}) + \frac{\partial g}{\partial V_{m,h}}\bigg|^{*}(V_{m,h} - V^{*}_{m,h}) \end{aligned} \tag{3.45}$$

$$\begin{aligned} Q^{L}_{mn,f} = h^{*} &+ \frac{\partial h}{\partial P_{mn,f}}\bigg|^{*}(P_{mn,f} - P^{*}_{mn,f}) + \frac{\partial h}{\partial P_{mn,h}}\bigg|^{*}(P_{mn,h} - P^{*}_{mn,h}) \\ &+ \frac{\partial h}{\partial Q_{mn,f}}\bigg|^{*}(Q_{mn,f} - Q^{*}_{mn,f}) + \frac{\partial h}{\partial Q_{mn,h}}\bigg|^{*}(Q_{mn,h} - Q^{*}_{mn,h}) \quad \forall mn \in L, f \in F \\ &+ \frac{\partial g}{\partial V_{m,f}}\bigg|^{*}(V_{m,f} - V^{*}_{m,f}) + \frac{\partial g}{\partial V_{m,h}}\bigg|^{*}(V_{m,h} - V^{*}_{m,h}) \end{aligned} \tag{3.46}$$

Hence, the complete LP model is given by (3.47).

$$\begin{aligned} &\min \alpha \\ &\text{subject to } (3.31)-(3.33), (3.41), (3.45), \text{and } (3.46) \end{aligned} \tag{3.47}$$

3.2.3 Performance and Accuracy

Two LP formulations to determine the steady-state operation point of an unbalanced network via mathematical optimization were presented. These representations are the base of the complete mathematical optimization framework for the distribution network operation. Different objectives related to technical and/or economic constraints can be pursued embedding these formulations in multi-period and multi-scenario optimization (see Appendix 2). Therefore, the quality of studies developed hereinafter will rely on their level of accuracy.

The performance and accuracy of both formulations is evaluated in the IEEE123-node test system [11]. All LP models were written in the mathematical language AMPL [12], and solved using CPLEX [3]. The case study had the following characteristics:

- The whole conventional demand of the distribution network was 1.62 MVA (40.61%), 1.05 MVA (26.36%), and 1.32 MVA (33.03%), connected to phases A, B, and C, respectively.
- All loads were connected in wye configuration.
- All demands were considered as constant power loads.

The LP formulations presented (3.17) and (3.44) are expressed as shown in (3.48) and (3.49), aiming to minimize the total active power generation; considering nominal voltage at the substation node. Moreover, as the accuracy of both unbalanced formulations depends on the precision of the assumed operation point (i.e., V^{re^*}, V^{im^*} for the current-based formulation, and P^L and Q^L for the power-based formulation), a two-stage approach was used for both formulations to obtain a better approximation for the operation point (see Appendix 3).

$$\begin{gathered}\min \sum_{f \in F}\left(V_{S,f}^{re} I_{S,f}^{Gre}+V_{S,f}^{im} I_{S,f}^{Gim}\right) \\ \text{subject to}: (3.6)-(3.9), (3.15), \text{and} (3.16)\end{gathered} \tag{3.48}$$

$$\begin{gathered}\min \sum_{f \in F} P_{S,f}^{G} \\ \text{subject to } (3.31) \text{ and } (3.41)-(3.43)\end{gathered} \tag{3.49}$$

A comparison of the two methods (Current-based and power-based power flow) was made analyzing the voltage magnitude profile obtained from each when compared to the one obtained from the solution of a conventional power flow. To solve this conventional power flow, the specialized software OpenDSS [13] was selected. For both formulations, Table 3.1 shows the maximum error percentage in the voltage magnitude, for each phase, compared against the OpenDSS; as well as the minimum voltage magnitude in the system.

Although both formulations show high accuracy when compared with OpenDSS results, it can be seen from Table 3.1, that the current-based LP formulation outperforms the power-based representation. This is an important fact to be taken

Table 3.1 Comparison of the LP formulations against OpenDSS

Phase	A		B		C	
LP formulation	Current-based	Power-based	Current-based	Power-based	Current-based	Power-based
Error (%)	0.01	0.02	0.01	0.05	0.11	0.30
Vmin (pu)	0.8996	0.8997	0.9599	0.9595	0.9241	0.9223

under consideration by the distribution network optimizer when choosing one LP formulation for an electric distribution network optimization algorithm. Nevertheless, the complexity due to troublesome constraints associated with operational limits and the inclusion of different technologies and devices should be thoroughly analyzed.

3.3 Operational Constraints

The LP formulations presented in (3.17) and (3.44) are expected to serve as the central engine of optimization analysis, mathematically formalizing decision–making processes regarding several objectives. Hereby, an essential component of any optimization strategy or algorithm related to electricity distribution is the service quality. Although several electrical quantities can be measured and limited to guarantee good quality in the service, voltage magnitude limits and thermal limits in conductors and transformers are the most commonly used in steady-state studies to ensure the proper operation of the electric distribution network. Therefore, the mathematical representation of these limits and their inclusion in the LP formulations are presented below.

3.3.1 Voltage Magnitude

Ensuring a good quality service in the electric distribution network, the voltage magnitude is limited within a range established by regulatory policies. This range is mathematically expressed as shown in (3.50), in terms of the minimum and maximum values of the voltage magnitude ($\underline{V}$ and $\bar{V}$, respectively). Therefore, the inclusion of (3.50) in the LP formulations is presented below.

$$\underline{V} \leq \left|\vec{V}\right| \leq \bar{V} \tag{3.50}$$

Current-Based Representation—Voltage Magnitude Limits: The current-based representation is written in terms of the currents and voltages real and imaginary parts. Hence, (3.50) is rewritten in (3.51), limiting the square power of the voltage magnitude. Nevertheless, (3.51) presents nonlinearities which have to be dealt with in order to include this limit in the LP model.

$$\underline{V}^2 \leq V_{n,f}^{re2} + V_{n,f}^{im2} \leq \bar{V}^2 \quad \forall n \in N, f \in F \tag{3.51}$$

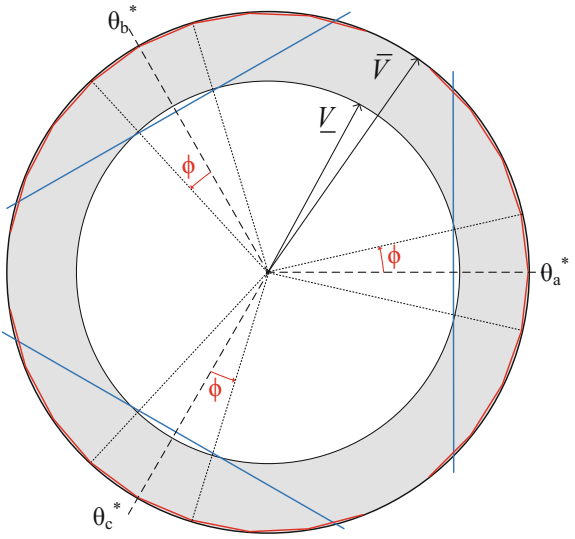

Fig. 3.4 Constraints for voltage limits in the current-based formulation

To reach a linear approximation for (3.51), a set of linear constraints limiting the feasible region for the voltage real and imaginary components is implemented. Figure 3.4 depicts the sets of lines used to approximate the upper and lower voltage limits (red lines and blue lines, respectively). In each phase, the upper limit is replaced by a set of $2 * \ell$ line segments; where ℓ lines are built clockwise starting from an estimated operation angle θ^*, and ℓ lines are built counterclockwise. For the lower limit, a single line is used for each phase also built around θ^*. Equation (3.52) and (3.53) are the mathematical expressions for the linear approximations of the upper and lower voltage limits, respectively.

$$V_{n,f}^{im} \leq \frac{\sin(\varphi_{n,f,i}^{+}) - \sin(\varphi_{n,f,i}^{-})}{\cos(\varphi_{n,f,i}^{+}) - \cos(\varphi_{n,f,i}^{-})} \left[V_{n,f}^{re} - \bar{V} \cos(\varphi_{n,f,i}^{-}) \right] + \bar{V} \sin(\varphi_{n,f,i}^{-}) \quad \forall i \in -\ell \ldots \ell, n \in N, f \in F \tag{3.52}$$

$$V_{n,f}^{im} \leq \frac{\sin(\varphi_{n,f}^{o+}) - \sin(\varphi_{n,f}^{o-})}{\cos(\varphi_{n,f}^{o+}) - \cos(\varphi_{n,f}^{o-})} \left[V_{n,f}^{re} - \underline{V} \cos(\varphi_{n,f}^{o+}) \right] + \underline{V} \sin(\varphi_{n,f}^{o+}) \quad \forall n \in N, f \in F \tag{3.53}$$

where $\varphi_{n,f,i}^{+} = \theta_{n,f}^{*} + \ell_i \phi$; $\varphi_{n,f,i}^{-} = \theta_{n,f}^{*} + (\ell_i - 1)\phi$; $\theta_{n,f}^{*}$ is the operation angle for bus n in phase f; ℓ_i is the i-element from the set of line segments; and ϕ is the angle of the arc corresponding to each line segment. Finally, $\varphi_{n,f,i}^{o+} = \theta_{n,f}^{*} + \phi$; and $\varphi_{n,f,i}^{o-} = \theta_{n,f}^{*} - \phi$.

Power-Based Representation—Voltage Magnitude Limits: On the other hand, to include the voltage magnitude limits in the power-based representation, (3.50) is rewritten in order to limit the square power of the voltage magnitude, as shown in (3.54).

$$\underline{V}^2 \leq V_{n,f}^{sqr} \leq \bar{V}^2 \quad \forall n \in N, f \in F \tag{3.54}$$

3.3.2 Circuit Currents

Thermal limits are often the main constraint in electric distribution networks. Hence, a proper operation of the electric distribution network must maintain the current in all circuits within the conductor thermal limitations; i.e., the magnitude of the current in all circuits must be held under their ampacities. Constraint (3.55) shows the general mathematical expression for the current limit, which is added to each LP formulation as

$$\left|\vec{I}\right| \leq \bar{I} \tag{3.55}$$

Current-Based Representation—Circuit Current Limits: Similar to the voltage magnitude limit, (3.55) is squared and expressed in terms of the real and imaginary parts of the circuit currents, as shown in (3.56). Later, the nonlinearities are avoided through a piecewise linearization technique, reaching a linear expression for the circuit current limit in terms of the real and imaginary parts of the current (3.57).

$$I_{mn,f}^{re2} + I_{mn,f}^{im2} \leq \bar{I}_{mn}^2 \quad \forall mn \in L, f \in F \tag{3.56}$$

$$f\left(I_{mn,f}^{re}, \bar{I}, \Lambda\right) + f\left(I_{mn,f}^{im}, \bar{I}, \Lambda\right) \leq \bar{I}_{mn}^2 \quad \forall mn \in L, f \in F \tag{3.57}$$

Power-Based Representation—Circuit Current Limits: Analogous to (3.50), (3.58) must be added to the power-based LP formulation to limit the current in each circuit.

$$I_{mn,f}^{sqr} \leq \bar{I}_{mn}^2 \quad \forall mn \in L, f \in F \tag{3.58}$$

3.3.3 Transformer Capacity

In steady-state studies of the electric distribution network where different voltage levels are taken into account, thermal limits regarding the distribution and substation transformers are a key aspect. Therefore, the inclusion of the transformer capacity in the mathematical optimization framework for the distribution network operation is presented below. Hence, the mathematical expression (3.59) limiting the transformer apparent power must be fulfilled for each transformer.

$$\left|\vec{S}\right| \leq \bar{S} \tag{3.59}$$

Hereby, let $TR \subseteq N$ be the set of nodes where a transformer is installed; while $P_{\wp}^{TR}$ and $Q_{\wp}^{TR}$ the active and reactive power, respectively, for transformer $\wp$. Thus, the general expression for each transformer capacity is presented in (3.60), and linearized in (3.61) through piecewise linearization technique.

$$P_{\wp}^{TR2} + Q_{\wp}^{TR2} \leq \overline{S_{\wp}^{TR}}^2 \quad \forall \wp \in TR \tag{3.60}$$

$$f(P_{\wp}^{TR}, \overline{S_{\wp}^{TR}}, \Lambda) + f(Q_{\wp}^{TR}, \overline{S_{\wp}^{TR}}, \Lambda) \leq \overline{S_{\wp}^{TR}}^2 \quad \forall \wp \in TR \tag{3.61}$$

Current-Based Representation—Transformer Capacity: Besides (3.61), for the current-based formulation, $P_{\wp}^{TR}$ and $Q_{\wp}^{TR}$ have to be calculated. Equations (3.62) and (3.63) calculate, for transformer $\wp$, the active and reactive powers in terms an operation point for the real and imaginary voltages $\left(V_{\wp,f}^{re/im*}\right)$ and the currents $\left(I_{\wp,f}^{re/im}\right)$ at the secondary windings.

$$P_{\wp}^{TR} = \sum_{f \in F} V_{\wp,f}^{re^*} I_{\wp,f}^{re} + V_{\wp,f}^{im^*} I_{\wp,f}^{im} \quad \forall \wp \in TR \tag{3.62}$$

$$Q_{\wp}^{TR} = \sum_{f \in F} -V_{\wp,f}^{re^*} I_{\wp,f}^{im} + V_{\wp,f}^{im^*} I_{\wp,f}^{re} \quad \forall \wp \in TR \tag{3.63}$$

Power-Based Representation—Transformer Capacity: Likewise, for the power-based formulation, (3.64) and (3.65) show the mathematical expression for $P_{\wp}^{TR}$ and $Q_{\wp}^{TR}$ in terms of the active an reactive power flowing through each phase of the transformer $\left(P_{\wp,f}\right.$ and $Q_{\wp,f}$, respectively).

$$P_{\wp}^{TR} = \sum_{f \in F} P_{\wp,f} \quad \forall \wp \in TR \tag{3.64}$$

$$Q_{\wp}^{TR} = \sum_{f \in F} Q_{\wp,f} \quad \forall \wp \in TR \tag{3.65}$$

Finally, the complete LP formulations, considering operational limits are presented in (3.66) and (3.67), for the current-based and power-based representations, respectively.

$$\min \alpha$$
$$\text{subject to} : (3.6) - (3.9), (3.15), (3.16), (3.52), (3.53), (3.57), \text{and} (3.61) - (3.63) \tag{3.66}$$

$$\min \alpha$$
$$\text{subject to} : (3.31), (3.41) - (3.43), (3.54), (3.58), (3.61), (3.64), \text{and} (3.65) \tag{3.67}$$

3.4 Load Representation

Nowadays, electric distribution networks must deal with social, technical and environmental challenges in order to successfully satisfy present-day consumers. The world's electrical energy consumption is expected to have an annual growth rate of about 2.2% until 2040 [14], which will substantially impact the operation of future networks. Hence, network operators are continuously challenged as they are in charge of meeting customer demands and optimize energy sources, while guaranteeing a reliable service. As a result, improvements in the network load modelling are continuously demanded within the grid operator efforts for predicting system behavior.

Besides the rapid growth of the conventional demand, electric distribution networks face issues related to the progressive integration of new technologies. The rise of new loads (e.g., electric vehicles), which cannot be pigeonholed in traditional classifications, require a special attention. Thus, this section presents the load modelling and the inclusion of special loads within the mathematical optimization framework.

3.4.1 Type of Loads: Voltage Dependent Load Models

In electric distribution networks, loads are traditionally classified as residential, industrial or commercial. This rough classification was elaborated in order to group

loads that share features related to usage patterns. These well-studied patterns are commonly affected by factors such as location, weather, cultural habits, and type of human works. However, since large concentrated loads called for detailed classifications and special representation in order to determine operational characteristics, studies have been performed aiming to achieve a more precise categorization for different types of loads [15]. Hereby, a new classification following the voltage dependency of the actual loads becomes more important in the representation as the network gets closer to individual loads. The demand of a distribution network is classified into loads that can be represented as

- constant power loads,
- constant impedance loads,
- constant current loads, or
- a combination of those.

Although load modelling in electric distribution networks is a well-studied topic, approached by several researches related to voltage and angular system stability, this issue has to be also taken into account on decision-making algorithms related to the steady-state operation of the grid. As discussed in [16–18], the effectiveness of several mathematical models in electric distribution networks is highly dependent on the accuracy of the load representation. Dependence on the voltage magnitude and frequency is considered in the load models; mathematically, this dependence can be represented by static and dynamic load models described by the traditional ZIP model. In this regards, two static models are commonly studied for the representation of the active and reactive demanded powers (P^D and Q^D, respectively): the polynomial load model and the exponential load model shown in (3.68) and (3.69), respectively [19].

$$\begin{aligned} P^D &= P^o\left(P^{Zo}\frac{V^2}{V^{o^2}} + P^{Io}\frac{V}{V^o} + P^{Po}\right) \\ Q^D &= Q^o\left(Q^{Zo}\frac{V^2}{V^{o^2}} + Q^{Io}\frac{V}{V^o} + Q^{Po}\right) \end{aligned} \tag{3.68}$$

$$\begin{aligned} P^D &= P^o\left(\frac{V}{V^o}\right)^{\alpha}\frac{1+K_{pf}(f_r - f_r^o)}{f_r^o} \\ Q^D &= Q^o\left(\frac{V}{V^o}\right)^{\beta}\frac{1+K_{qf}(f_r - f_r^o)}{f_r^o} \end{aligned} \tag{3.69}$$

where P^o, Q^o, and V^o, are the nominal active and reactive power and bus voltage, respectively. P^{Zo}, P^{Io}, and P^{Po}, are the active power percentage of the total load classified as constant impedance, constant current, and constant power, respectively. Likewise, Q^{Zo}, Q^{Io}, and Q^{Po}, are the reactive power percentage for constant impedance, constant current, and constant power, respectively. In the polynomial load model (3.68), the loads are treated as a combination of constant impedance

constant current and/or constant power; hence the sum of these coefficients will represent the total load, as shown in (3.70). On the other hand, in the exponential load model (3.69) the load voltage dependency is generalized, and the demanded active and reactive powers vary according to the voltage exponents α and β. These voltage exponents depend on the type and composition of the load.

$$\begin{aligned} P^{Zo} + P^{Io} + P^{Po} &= 1 \\ Q^{Zo} + Q^{Io} + Q^{Po} &= 1 \end{aligned} \tag{3.70}$$

Moreover, f_r represents the frequency of the bus voltage and f_r^o represents the nominal frequency. The coefficients K_{pf} and K_{qf} are the frequency sensitivities for the active and reactive power loads, respectively. Nevertheless, for the exponential model the effects associated with frequency may be disregarded, as shown in (3.71). Hence, with an appropriate adjustment of the constants α and β the model can be restricted to the steady-state analysis case (i.e., dependence directly on the voltage magnitude). Appropriate values for these constants may be found in previous works, such as [20].

$$\begin{aligned} P^D &= P^o \left(\frac{V}{V^o} \right)^{\alpha} \\ Q^D &= Q^o \left(\frac{V}{V^o} \right)^{\beta} \end{aligned} \tag{3.71}$$

In some decision-making processes for electric distribution networks, the load voltage dependency is a key aspect of the suitable representation of the network operation, e.g., volt-var control. Hence, they must be included in the LP formulations presented in (3.17) and (3.44), where the demanded active and reactive powers were considered as constant values.

Current-Based Representation—Polynomial load model: In order to include the load voltage dependency in the LP problem presented in (3.17), the values of the demanded powers have to be replaced by (3.68) in (3.13) and (3.14). Therefore, the expressions representing the functions g and h are presented in (3.72) and (3.73).

$$\begin{aligned} g = & \frac{P^o_{n,f} V^{re}_{n,f}}{V^{re2}_{n,f} + V^{im2}_{n,f}} \left(\frac{P^{Zo}_{n,f}}{V_n^{o^2}} \left(V^{re2}_{n,f} + V^{im2}_{n,f} \right) + \frac{P^{Io}_{n,f}}{V^o_n} \sqrt{\left(V^{re2}_{n,f} + V^{im2}_{n,f} \right)} + P^{Po}_{n,f} \right) \\ & + \frac{Q^o_{n,f} V^{im}_{n,f}}{V^{re2}_{n,f} + V^{im2}_{n,f}} \left(\frac{Q^{Zo}_{n,f}}{V_n^{o^2}} \left(V^{re2}_{n,f} + V^{im2}_{n,f} \right) + \frac{Q^{Io}_{n,f}}{V^o_n} \sqrt{\left(V^{re2}_{n,f} + V^{im2}_{n,f} \right)} + Q^{Po}_{n,f} \right) \\ & \forall n \in N, f \in F \end{aligned} \tag{3.72}$$

$$h = \frac{P^{o}_{n,f} V^{im}_{n,f}}{V^{re2}_{n,f} + V^{im2}_{n,f}} \left(\frac{P^{Zo}_{n,f}}{V^{o^2}_{n}} \left(V^{re2}_{n,f} + V^{im2}_{n,f} \right) + \frac{P^{Io}_{n,f}}{V^{o}_{n}} \sqrt{\left(V^{re2}_{n,f} + V^{im2}_{n,f} \right)} + P^{Po}_{n,f} \right) - \frac{Q^{o}_{n,f} V^{re}_{n,f}}{V^{re2}_{n,f} + V^{im2}_{n,f}} \left(\frac{Q^{Zo}_{n,f}}{V^{o^2}_{n}} \left(V^{re2}_{n,f} + V^{im2}_{n,f} \right) + \frac{Q^{Io}_{n,f}}{V^{o}_{n}} \sqrt{\left(V^{re2}_{n,f} + V^{im2}_{n,f} \right)} + Q^{Po}_{n,f} \right) \quad \forall n \in N, f \in F \tag{3.73}$$

Current-Based Representation—Exponential load model: Likewise, to include the exponential load model in (3.17), (3.13) and (3.14) have to be rewritten, as shown in (3.74) and (3.75).

$$g = P^{o}_{n,f} \frac{V^{re}_{n,f}}{V^{\alpha_{n,f}}_{o}} \left(V^{re^2}_{n,f} + V^{im^2}_{n,f} \right)^{\frac{\alpha_{n,f}}{2}-1} + Q^{o}_{n,f,t} \frac{V^{im}_{n,f}}{V^{\beta_{n,f}}_{o}} \left(V^{re^2}_{n,f} + V^{im^2}_{n,f} \right)^{\frac{\beta_{n,f}}{2}-1} \quad \forall n \in N, f \in F \tag{3.74}$$

$$h = P^{o}_{n,f} \frac{V^{im}_{n,f}}{V^{\alpha_{n,f}}_{o}} \left(V^{re^2}_{n,f} + V^{im^2}_{n,f} \right)^{\frac{\alpha_{n,f}}{2}-1} - Q^{o}_{n,f,t} \frac{V^{re}_{n,f}}{V^{\beta_{n,f}}_{o}} \left(V^{re^2}_{n,f} + V^{im^2}_{n,f} \right)^{\frac{\beta_{n,f}}{2}-1} \quad \forall n \in N, f \in F \tag{3.75}$$

Power-Based Representation—Polynomial load model: For the power-based linear representation shown in (3.44), the expressions for the demanded power (3.68) are directly added to the formulation; notwithstanding, the nonlinearities of these equations must be dealt with, as shown in (3.76) and (3.77).

$$P^{D}_{n,f} = P^{o}_{n,f} \left(P^{Zo}_{n} \frac{V^{sqr}_{n,f}}{V^{o^2}_{n}} + P^{Io}_{n} \frac{V^{sqr}_{n,t}}{V^{*}_{n,t} V^{o}_{n}} + P^{Po}_{n} \right) \quad \forall n \in N, f \in F \tag{3.76}$$

$$Q^{D}_{n,f} = Q^{o}_{n,f} \left(Q^{Zo}_{n} \frac{V^{sqr}_{n,f}}{V^{o^2}_{n}} + Q^{Io}_{n} \frac{V^{sqr}_{n,t}}{V^{*}_{n,t} V^{o}_{n}} + Q^{Po}_{n} \right) \quad \forall n \in N, f \in F \tag{3.77}$$

Hence, the complete LP formulation, considering the polynomial model for the load voltage dependency, is given by (3.78).

$$\begin{aligned} &\min \alpha \\ &\text{subject to : } (3.31) - (3.33), (3.41), (3.45), (3.46), (3.74), \text{and} (3.75) \end{aligned} \tag{3.78}$$

Power-Based Representation—Exponential load model: Finally, to include the exponential load model in the power-based LP formulation, expressions (3.71) are added. To avoid the nonlinearities associated to these expressions, (3.71) is rewritten as shown in (3.79) and (3.80).

$$P^D_{n,f} = P^o_{n,f}\left(\frac{V^{sqr}_{n,f}}{V^{o^2}_n}\right)^{\frac{\alpha_{n,f}}{2}} \quad \forall n \in N, f \in F \tag{3.79}$$

$$Q^D_{n,f} = Q^o_{n,f}\left(\frac{V^{sqr}_{n,f}}{V^{o^2}_n}\right)^{\frac{\beta_{n,f}}{2}} \quad \forall n \in N, f \in F \tag{3.80}$$

Later, Taylor's approximation is applied to linearize (3.79) and (3.80).

$$P^D_{n,f} = P^o_{n,f}\left(\frac{V^{sqr*}_{n,f}}{V^{o^2}_n}\right)^{\frac{\alpha_{n,f}}{2}} + \frac{\alpha_{n,f}}{2}\frac{P^o_{n,f}}{\left(V^o_n\right)^{\frac{\alpha_{n,f}}{2}}} V^{sqr*\left(\frac{\alpha_{n,f}}{2}-1\right)}_{n,f}\left(V^{sqr}_{n,f} - V^{sqr*}_{n,f}\right) \quad \forall n \in N, f \in F \tag{3.81}$$

$$Q^D_{n,f} = Q^o_{n,f}\left(\frac{V^{sqr*}_{n,f}}{V^{o^2}_n}\right)^{\frac{\beta_{n,f}}{2}} + \frac{\beta_{n,f}}{2}\frac{Q^o_{n,f}}{\left(V^o_n\right)^{\frac{\beta_{n,f}}{2}}} V^{sqr*\left(\frac{\beta_{n,f}}{2}-1\right)}_{n,f}\left(V^{sqr}_{n,f} - V^{sqr*}_{n,f}\right) \quad \forall n \in N, f \in F \tag{3.82}$$

Therefore, the complete LP formulation, considering the exponential load voltage dependency model, is given by (3.83).

$$\begin{gathered}\min \alpha \\ \text{subject to : } (3.31)-(3.33), (3.41), (3.45), (3.46), (3.81), \text{and } (3.82)\end{gathered} \tag{3.83}$$

3.4.2 Special Loads: Plug-In Electric Vehicles

A large number of EVs is expected to be integrated to the transport sector in the upcoming years, as an to environmental concerns related to the reduction of greenhouse gas emissions [21]. From the point of view of the customers, EVs represent an economical option in response to high fuel costs. On the other hand, for the electric distribution network, EVs represent an additional load which need to be attended, increasing the conventional demand in several ways, depending on the charging place [22]. Hence, EVs are new loads in networks which have to be taken into account in optimization studies for the grid.

EVs recharge their batteries from the distribution network, and an uncontrolled charging of large fleets can cause overloads, voltage limit violations, and excessive

energy losses [23]. Hence, the EV charging coordination (EVCC) problem have to be tackled as part of the distribution network operation, and has received much attention in recent years [24, 25]. Furthermore, the ability of EVs to inject power into the grid (also known as vehicle-to-grid (V2G) technology), providing ancillary services to the network, also represent a highly studied subject [25, 26].

In order to include the EVCC within the electric distribution network optimization framework, let EV be the set of EVs plugged into the grid. P_e^{EV} is the power injected/drawn by EV e, and it is equal to the sum of the maximum charging and discharging powers ($\bar{P}_e^{EV+}$ and $\bar{P}_e^{EV-}$, respectively) multiplied by the binary variables y_e and z_e, which represent the charging or discharging state, as shown in (3.84). Moreover, (3.85) ensures only one action for the EV (e.g., charging, discharging, or idle). Due to the binary nature of these variables, a MILP model is obtained as the result of their inclusion.

$$P_e^{EV} = \bar{P}_e^{EV+} y_e - \bar{P}_e^{EV-} z_e \quad \forall e \in EV \tag{3.84}$$

$$y_e + z_e \leq 1 \quad \forall e \in EV \tag{3.85}$$

On the other hand, EVs storage capacity also needs to be taken into account, i.e., maximum energy limit ($\bar{E}_e^{EV}$) and, for V2G applications, the maximum depth of discharge (DoD) must be always fulfilled. Hence, if an EV is charged/discharged constantly at P_e^{EV} during a time interval Δt, (3.86) ensures that the state of charge (SOC) is always maintained between the pre-established limits.

$$\min\left(E_e^{EVi}, \bar{E}_e^{EV} DoD\right) \leq E_e^{EVi} + \Delta t(\bar{P}_e^{EV+} y_e \eta_e^{EV+} - \bar{P}_e^{EV-} z_e \eta_e^{EV-}) \leq \bar{E}_e^{EV} \quad \forall e \in EV \tag{3.86}$$

where E_e^{EVi} is the initial SOC for EV e; while, η_e^{EV+} and η_e^{EV-} are the charging and discharging efficiencies, respectively.

The interaction of the EVs with the grid is integrated in the steady-state operation as follows:

Current-Based Representation—EV: Eqs. (3.87) and (3.88) represent the EV active and reactive powers in terms of the voltage operation point (V_e^*) where the EV is plugged, and the EV current (I_e^{EVre}). Considering that EVs will only exchange active power. Moreover, (3.89) and (3.90) are the extensions of (3.8) and (3.9) taking into account the EV current injection in each node.

$$P_e^{EV} = V_e^{re*} I_e^{EVre} + V_e^{im*} I_e^{EVim} \quad \forall e \in EV \tag{3.87}$$

$$0 = -V_e^{re*} I_e^{EVim} + V_e^{im*} I_e^{EVre} \quad \forall e \in EV \tag{3.88}$$

$$I_{m,f}^{Gre} + \sum_{km\in L} I_{km,f}^{re} - \sum_{mn\in L} I_{mn}^{re} - \left(\sum_{km\in L} B_{km,f} + \sum_{mn\in L} B_{mn,f}\right)\frac{V_{m,f}^{im}}{2} = I_{m,f}^{Dre} + \sum_{e\in EV} I_e^{EVre}\gamma_{e,m,f} \quad \forall m \in N, f \in F \tag{3.89}$$

$$I_{m,f}^{Gim} + \sum_{km\in L} I_{km,f}^{im} - \sum_{mn\in L} I_{mn}^{im} - \left(\sum_{km\in L} B_{km,f} + \sum_{mn\in L} B_{mn,f}\right)\frac{V_{m,f}^{re}}{2} = I_{m,f}^{Dim} + \sum_{e\in EV} I_e^{EVim}\gamma_{e,m,f} \quad \forall m \in N, f \in F \tag{3.90}$$

where $\gamma_{x,m,f}$ is a binary parameter that takes a value of 1 if the device x is connected at node m and phase f.

Power-Based Representation—EV: For this formulation, (3.91) represents the active power balance in each node, taking into account the EV active power injection/consumption.

$$\sum_{km\in L} P_{km,f} - \sum_{mn\in L}\left(P_{mn,f} + P_{mn,f}^{L}\right) + P_{m,f}^{G} = P_{m,f}^{D} + \sum_{e\in EV} P_e^{EV}\gamma_{e,m,f} \quad \forall m \in N, f \in F \tag{3.91}$$

Therefore, the complete MILP formulations for an unbalanced network, considering EV operation is presented in (3.92) and (3.93) for the current-based and power-based formulations, respectively.

$$\begin{gathered}\min \alpha \\ \text{subject to}: (3.6)-(3.9), (3.15), (3.16), \text{and} (3.84)-(3.90)\end{gathered} \tag{3.92}$$

$$\begin{gathered}\min \alpha \\ \text{subject to}: (3.31), (3.41)-(3.43), (3.84)-(3.86), \text{and} (3.91)\end{gathered} \tag{3.93}$$

3.5 Distributed Generation

Since the decade of 2000s, distributed generation has continuously grown among electric distribution networks, motivated by economic, environmental, technical, and market related features [27, 28]. Due to the flexibility of DG as a power source, distribution networks have been transformed from a passive network to an active network. Nowadays, DG plays an important role in the operation, structure and

design of networks; therefore, several researches have been developed to model the integration of DG units in the network operation [29–31].

DG units are integrated into the electric distribution network in places that were not originally adapted to connect them can create several problems for distribution networks in terms of stability and power quality; particularly, when large amounts of DG units are connected to high impedance networks. In addition, integrating renewable sources of DG, such as wind or solar power, can mean new challenges to the network operation. Furthermore, according to the capacity of the DG units, the network can become an active one, attending loads without the need of the energy purchased from the main grid. Therefore, the inclusion of the DG in the study of the network operation is imperative [2].

On the other hand, DG can also offer several advantages to the electric distribution network, i.e., improving system reliability, reducing energy losses, reducing transmission and distribution line costs, and alleviating congestion in the grid. Moreover, the installation of small-scale DG units, close to loads, may delay or avoid investments in additional transmission or distribution infrastructure. In addition, certain types of DGs also have the ability to offer ancillary services, such as reactive power support, voltage control, and frequency control.

Typically, in mathematical representations for DG units, the models of synchronous generators (SiGs), induction generators (IGs), and doubly-fed induction generators (DFIGs) are disregarded. DG units are commonly modelled by a simple representation and coupling elements are not detailed. Hence, a simple mathematical representation is presented in (3.94)–(3.97) for the generation limits of DG units.

$$(P_n^{DG})^2 + (Q_n^{DG})^2 \leq (\bar{S}_n^{DG})^2 \quad \forall n \in DG \tag{3.94}$$

$$Q_n^{DG} \leq P_n^{DG} \tan(\arccos(pf_n^{DG})) \quad \forall n \in DG \tag{3.95}$$

$$\underline{Q_n^{DG}} \leq Q_n^{DG} \leq \overline{Q_n^{DG}} \quad \forall n \in DG \tag{3.96}$$

$$P_n^{DG} \geq 0 \quad \forall n \in DG \tag{3.97}$$

where $DG \subseteq N$ represents the set of nodes in which a DG unit is connected. P_n^{DG} and Q_n^{DG} are the active and reactive powers of DG unit n; while, pf_n^{DG} is the minimum power factor, $\underline{Q}_n^{DG}$ and $\bar{Q}_n^{DG}$ are the minimum and maximum reactive power limits, and, S_n^{DG} is the maximum apparent power. Therefore, (3.94) shows the nonlinear representation for the apparent power limit, and it is approximated in (3.98) via a piecewise linearization technique. Constraints (3.95) and (3.96) limit the reactive power in terms of the power factor and the maximum and minimum reactive power limits, respectively. Finally, (3.97) ensures non-negativity for the active power of the DG unit.

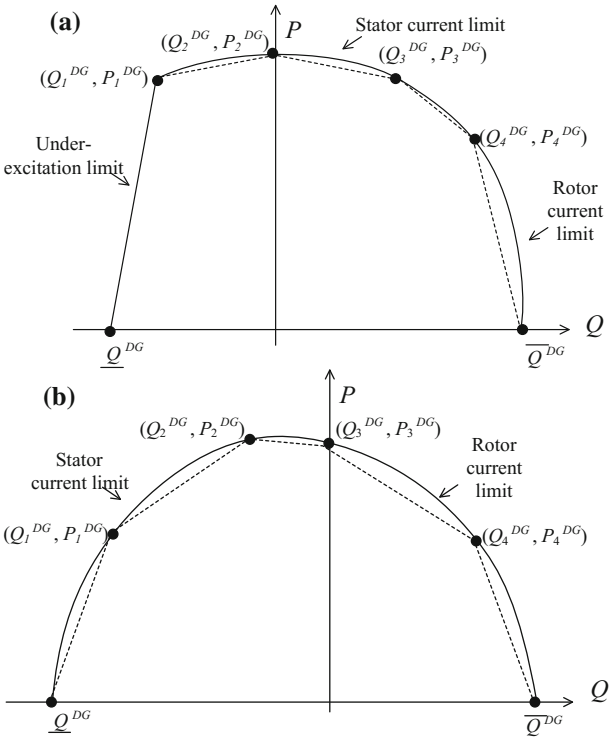

Fig. 3.5 Capability curves: **a** DFIG and **b** SiG [29]

$$f\left(P_n^{DG}, \overline{P_n^{DG}}, \Lambda\right) + f\left(Q_n^{DG}, \overline{Q_n^{DG}}, \Lambda\right) \leq (\bar{S}_n^{DG})^2 \quad \forall n \in DG \tag{3.98}$$

On the other hand, an improved and realistic model for DG units, considering the capability curves (see Fig. 3.5) for SiGs and DFIGs is presented in [29]. These types of generators are widely used in DG applications, e.g., wind turbines, biomass-based CHP generation systems, and small hydroelectric plants.

Figure 3.5 defines the points $(Q_{1,n}^{DG}, P_{1,n}^{DG}), (Q_{2,n}^{DG}, P_{2,n}^{DG}), (Q_{3,n}^{DG}, P_{3,n}^{DG})$, and $(Q_{4,n}^{DG}, P_{4,n}^{DG})$, which are used to obtain linear expressions for the DG operation constraints, as

$$P_n^{DG} \leq \frac{P_{1,n}^{DG}}{Q_{1,n}^{DG} - \underline{Q}_n^{DG}} (Q_n^{DG} - \underline{Q}_n^{DG}) \quad \forall n \in DG \tag{3.99}$$

$$P_n^{DG} \leq \frac{P_{2,n}^{DG} - P_{1,n}^{DG}}{Q_{2,n}^{DG} - Q_{1,n}^{DG}} (Q_n^{DG} - Q_{2,n}^{DG}) + P_{2,n}^{DG} \quad \forall n \in DG \tag{3.100}$$

Table 3.2 Linearization points for the linearization of distributed generators capability curves [29]

	SiG	DFIG
$(Q_{1,n}^{DG}, P_{1,n}^{DG})$	the intersection between the under-excitation and armature current limits	half of the arc of the armature current limit between points $(\underline{Q}_n^{DG}, 0)$ and $(Q_{2,n}^{DG}, P_{2,n}^{DG})$
$(Q_{2,n}^{DG}, P_{2,n}^{DG})$	the intersection between the armature current limit and the P axis	the intersection between the armature current and field current limits,
$(Q_{3,n}^{DG}, P_{3,n}^{DG})$	half of the arc of the armature current limit between points $(Q_{2,n}^{DG}, P_{2,n}^{DG})$ and $(Q_{4,n}^{DG}, P_{4,n}^{DG})$	the intersection between the field current limit and the P axis
$(Q_{4,n}^{DG}, P_{4,n}^{DG})$	the intersection between the armature current and field current limits	the half of the arc of the field current limit between points $(Q_{3,n}^{DG}, P_{3,n}^{DG})$ and $(\bar{Q}_n^{DG}, 0)$

$$P_n^{DG} \leq \frac{P_{3,n}^{DG} - P_{2,n}^{DG}}{Q_{3,n}^{DG} - Q_{2,n}^{DG}} (Q_n^{DG} - Q_{3,n}^{DG}) + P_{3,n}^{DG} \quad \forall n \in DG \tag{3.101}$$

$$P_n^{DG} \leq \frac{P_{4,n}^{DG}}{Q_{4,n}^{DG} - \bar{Q}_n^{DG}} (Q_n^{DG} - \bar{Q}_n^{DG}) \quad \forall n \in DG \tag{3.102}$$

Table 3.2 shows how these points were obtained for each type of generator.

Moreover, the power injection of the DG units connected in the system is integrated in the electric distribution network steady-state formulations as follows:

Current-Based Representation—DG Units: Assuming three-phase DG units, (3.103) and (3.104) represent the DG unit active and reactive powers in terms of the voltage operation point and their currents $\left(I_{n,f}^{DG}\right)$. Finally, the current injection due to DG units is included in the current balance for each node, as:

$$P_n^{DG}/3 = V_{n,f}^{re*} I_{n,f}^{DGre} + V_{n,f}^{im*} I_{n,f}^{DGim} \quad \begin{matrix} \forall n \in DG, \\ f \in F \end{matrix} \tag{3.103}$$

$$Q_n^{DG}/3 = -V_{n,f}^{re*} I_{n,f}^{DGim} + V_{n,f}^{im*} I_{n,f}^{DGre} \quad \begin{matrix} \forall n \in DG, \\ f \in F \end{matrix} \tag{3.104}$$

$$I_{m,f}^{Gre} + I_{m,f}^{DGre} + \sum_{km \in L} I_{km,f}^{re} - \sum_{mn \in L} I_{mn}^{re} - \left(\sum_{km \in L} B_{km,f} + \sum_{mn \in L} B_{mn,f} \right) \frac{V_{m,f}^{im}}{2} = I_{m,f}^{Dre} \quad \begin{matrix} \forall m \in N, \\ f \in F \end{matrix} \tag{3.105}$$

$$I_{m,f}^{Gim} + I_{m,f}^{DGim} + \sum_{km \in L} I_{km,f}^{im} - \sum_{mn \in L} I_{mn}^{im} - \left(\sum_{km \in L} B_{km,f} + \sum_{mn \in L} B_{mn,f} \right) \frac{V_{m,f}^{re}}{2} = I_{m,f}^{Dim} \quad \begin{matrix} \forall m \in N, \\ f \in F \end{matrix} \tag{3.106}$$

Power-Based Representation—DG Units: For this formulation, active and reactive powers are included in the power balance as:

$$\sum_{km \in L} P_{km,f} - \sum_{mn \in L} \left(P_{mn,f} + P_{mn,f}^{L} \right) + P_{m,f}^{G} + P_{m}^{DG}/3 = P_{m,f}^{D} \quad \forall m \in N, f \in F \tag{3.107}$$

$$\sum_{km \in L} Q_{km,f} - \sum_{mn \in L} \left(Q_{mn,f} + Q_{mn,f}^{L} \right) + Q_{m,f}^{G} + Q_{m}^{DG}/3 = Q_{m,f}^{D} \quad \forall m \in N, f \in F \tag{3.108}$$

Therefore, the complete LP formulations for an unbalanced network, considering DG units is presented by:

$$\begin{matrix} \min \alpha \\ \text{subject to : } (3.6) - (3.9), (3.15), (3.16), (3.95) - (3.98), \text{ and } (3.103) - (3.106) \end{matrix} \tag{3.109}$$

$$\begin{matrix} \min \alpha \\ \text{subject to : } (3.31), (3.41) - (3.43), (3.95) - (3.98), (3.107), \text{and } (3.108) \end{matrix} \tag{3.110}$$

for the current-based and power-based formulations, respectively.

3.5.1 Renewable DG

Different from the dispatchable DG, in which the electric distribution network operator controls the active and reactive powers injection for each DG unit, renewable generation depends on availability of renewable resources (e.g., wind speed and solar irradiance). Nowadays, renewable DG has taken an important role

in the decentralization of energy production [32]. Due to difficulties related to DG forecasting when it operates from renewable energy sources, additional considerations must be taken into account to properly include this type of DG into a distribution network optimization framework. Moreover, with the increase in penetration of these technologies, issues related to voltage profiles, energy losses, restoration actions, and network reinforcements have to be addressed.

In this regard, (3.111) represents an additional constraint for renewable DG units, and models an active power curtailment. This technique is used in order to avoid undesired levels of power injection from renewable sources which can lead to voltage rises and high energy losses [33, 34].

$$\hat{P}_n^{DG} = P_n^{DG} + \tilde{P}_n^{DG} \quad \forall n \in DG \tag{3.111}$$

where $\hat{P}_n^{DG}$ and $\tilde{P}_n^{DG}$ are the maximum available power and the power curtailment for DG unit n. Under this optimization scheme, $\hat{P}_n^{DG}$ will depend on the availability related to the renewable energy source (e.g., wind speed and solar irradiance); hence, multi-scenario approaches are mainly used to tackle this problems.

3.6 Energy Storage Devices

Energy storage systems have been foregrounded as an answer to conciliate time-difference between excessive generation and peak demand. In recent years, energy storage devices prices have declined, which in turn, raised the usage of these technologies in the electric distribution networks. For electric distribution, battery-based energy storage systems (BESS) are the most common type of storage. This is because other storage technologies such as super capacitors and flywheels are characterized by their high energy cost and are primarily applied on high power, short duration applications. Hence, due to the growth in the utilization of BESS and their constant interaction with renewable DG and EVs, their inclusion in the distribution network steady-state operation must be addressed [18, 35, 36].

3.6.1 BESS Operation

The BESS power drawn or injected from/to the grid must be taken into account in the steady-state operation of the system. Thus, let SD be the set of BESSs plugged into the grid. P_u^{SD} is the power injected/drawn by BESS u, and it is equal to the sum of two non-negative variables that represent the ESS charging and discharging powers (P_u^{SD+} and P_u^{SD-}, respectively), as shown in (3.112). Moreover, (3.113) and (3.114) limit the variables P_u^{SD+} and P_u^{SD-}, in terms of the BESS maximum charging/discharging power $\left(\bar{P}_u^{SD}\right)$ and the binary variables w_u and x_u.

Equation (3.115) ensures only one action for the BESS (e.g., charging, discharging, or idle). Due to the integer nature of these variables, once they are included in the distribution network optimization framework, one obtains a MILP problem.

$$P_u^{SD} = P_u^{SD+} - P_u^{SD-} \quad \forall u \in SD \tag{3.112}$$

$$0 \le P_u^{SD+} \le \bar{P}_u^{SD} w_u \quad \forall u \in SD \tag{3.113}$$

$$0 \le P_u^{SD-} \le \bar{P}_u^{SD} x_u \quad \forall u \in SD \tag{3.114}$$

$$w_u + x_u \le 1 \quad \forall u \in SD \tag{3.115}$$

On the other hand, BESS have physical constraints regarding their storage capacity, i.e., the maximum energy limit $\left(\bar{E}_u^{SD}\right)$ and the maximum DoD must be always fulfilled. Hence, if the P_u^{SD} is maintained during a time interval Δt, (3.116) keeps the BESS energy level between the pre-established limits.

$$\bar{E}_u^{SD} DoD \le E_u^{SDi} + \Delta t(P_u^{SD+}\eta_u^{+} - P_u^{SD-}\eta_u^{-}) \le \bar{E}_u^{SD} \quad \forall u \in SD \tag{3.116}$$

where E_u^{SDi} is the initial SOC for BESS u; while, η_u^{+} and η_u^{-} are the charging and discharging efficiencies, respectively.

The interaction of the BESSs with the grid is integrated in the steady-state operation as follows:

Current-Based Representation—BESS: Initially, in (3.117) and (3.118) the active and reactive powers injected or consumed by the BESS are expressed in terms of the voltage operation point $\left(V_u^{*}\right)$ where the BESS is connected and the BESS current $\left(I_u^{SDre}\right)$. Considering that BESSs will only inject/drawn active power. Moreover, (3.119) and (3.120) are the extensions of (3.8) and (3.9) taking into account the BESS current injection in each node.

$$P_u^{SD} = V_u^{re*} I_u^{SDre} + V_u^{im*} I_u^{SDim} \quad \forall u \in SD \tag{3.117}$$

$$0 = -V_u^{re*} I_u^{SDim} + V_u^{im*} I_u^{SDre} \quad \forall u \in SD \tag{3.118}$$

$$I_{m,f}^{Gre} + \sum_{km \in L} I_{km,f}^{re} - \sum_{mn \in L} I_{mn}^{re} - \left(\sum_{km \in L} B_{km,f} + \sum_{mn \in L} B_{mn,f}\right)\frac{V_{m,f}^{im}}{2} = I_{m,f}^{Dre} + \sum_{u \in SD} I_u^{SDre}\gamma_{u,m,f} \quad \forall m \in N, f \in F \tag{3.119}$$

$$I_{m,f}^{Gim} + \sum_{km \in L} I_{km,f}^{im} - \sum_{mn \in L} I_{mn}^{im} - \left(\sum_{km \in L} B_{km,f} + \sum_{mn \in L} B_{mn,f} \right) \frac{V_{m,f}^{re}}{2} = I_{m,f}^{Dim} + \sum_{u \in SD} I_u^{SDim} \gamma_{u,m,f} \quad \forall m \in N, f \in F \tag{3.120}$$

where $\gamma_{x,m,f}$ is a binary parameter that takes a value of 1 if the device x is connected at node m and phase f.

Power-Based Representation—BESS: For this formulation, (3.121) represents the active power balance in each node, taking into account the BESS active power injection/consumption.

$$\sum_{km \in L} P_{km,f} - \sum_{mn \in L} \left(P_{mn,f} + P_{mn,f}^{L} \right) + P_{m,f}^{G} = P_{m,f}^{D} + \sum_{u \in SD} P_u^{SD} \gamma_{u,m,f} \quad \forall m \in N, f \in F \tag{3.121}$$

Therefore, the complete MILP formulations for an unbalanced network, considering BESS is presented in (3.122) and (3.123) for the current-based and power-based formulations, respectively.

$$\begin{aligned} &\min \alpha \\ &\text{subject to : } (3.6)-(3.9), (3.15), (3.16), \text{and } (3.112)-(3.121) \end{aligned} \tag{3.122}$$

$$\begin{aligned} &\min \alpha \\ &\text{subject to : } (3.31), (3.41)-(3.43), (3.112)-(3.116), \text{and } (3.121) \end{aligned} \tag{3.123}$$

3.7 Voltage and Reactive Power Control Devices

Voltage optimization and reactive power control have been widely used in power systems as tools to improve energy efficiency and quality [16, 17]. In electric distribution networks, the management of voltage magnitudes variations together with the reactive power flows is known as volt-var control (VVC). The main objective of the VVC is to determine control actions for the devices related to voltage management and reactive power flow management. The classical devices controlled within a VVC scheme are on-load tap changers (OLTCs), voltage regulators (VRs), and switched capacitor banks (SCBs). Hence, the optimization of the VVC will pursue a proper distribution network operation, while maximizing or

minimizing an objective imposed by the distribution network operator, e.g., power loss reduction, minimization of voltage deviation, or maximization of energy efficiency.

In this framework the mathematical modeling for the optimization of the VVC problem is presented. A solution for the VVC problem will provide the number of enabled/disabled modules in every SCB, and the tap position for the OLTCs and VRs. Hence, the mathematical representation for the switchable SCBs, OLTCs, and VRs, are shown for both LP formulations. Due to the integer nature of the variables that model the operation of the VVC devices, the obtain formulations corresponds to a MILP problem.

3.7.1 Capacitor Banks

The inclusion of switchable SCBs in the electric distribution network operation will represent an injection of reactive power that will depend on the number of SCB modules enabled. Thus, let $CB \subseteq N$ be the set of nodes where a three-phase SCB is installed. B_n is an integer variable that represents the number of modules enabled from the SCB connected at node n; $\bar{B}_n$ is the maximum number of SCB modules; Q_n^{cb} is the reactive power delivered; and Q_n^{esp} is the reactive power capacity of each module. Equation (3.124) represents the reactive power injected by the modules of the switchable SCBs, while the maximum number of operating modules for each BC is modeled by (3.125).

$$Q_n^{cb} = B_n Q_n^{esp} \quad \forall n \in CB \tag{3.124}$$

$$0 \leq B_n \leq \bar{B}_n \quad \forall n \in CB \tag{3.125}$$

Furthermore, in a multi-period optimization where the SCB operations permitted along the entire time period must be limited, (3.126) must be taken into account.

$$\sum_{t \in T} \left| B_{n,t} - B_{n,t-1} \right| \leq \Delta^{cb} \quad \forall n \in CB \tag{3.126}$$

where T is the set of time intervals; $B_{n,t}$ is the number of modules enabled from the SCB connected at node n in time t; and Δ^{cb} is the maximum number of operations allowable over the time period.

The reactive power injection Q_n^{cb} is included in the steady-state operation of the distribution network as follows:

Current-Based Representation—Capacitor Banks: The active and reactive power of the switchable SCBs are represented by (3.127) and (3.128), considering that the value for the active power injection of every SCB will always be equal to zero.

Moreover, the current balances in each node are updated to include the injection due to the SCB reactive power, as shown in (3.129) and (3.130).

$$0 = V_{n,f}^{re*} I_{n,f}^{cbre} + V_{n,f}^{im*} I_{n,f}^{cbim} \quad \forall n \in CB, f \in F \tag{3.127}$$

$$\frac{Q_n^{cb}}{3} = -V_{n,f}^{re*} I_{n,f}^{cbim} + V_{n,f}^{im*} I_{n,f}^{cbre} \quad \forall n \in CB, f \in F \tag{3.128}$$

$$I_{m,f}^{Gre} + \sum_{km \in L} I_{km,f}^{re} - \sum_{mn \in L} I_{mn}^{re} - \left(\sum_{km \in L} B_{km,f} + \sum_{mn \in L} B_{mn,f} \right) \frac{V_{m,f}^{im}}{2} = I_{m,f}^{Dre} - I_{n,f}^{cbre} \quad \forall n \in N, f \in F \tag{3.129}$$

$$I_{m,f}^{Gim} + \sum_{km \in L} I_{km,f}^{im} - \sum_{mn \in L} I_{mn}^{im} - \left(\sum_{km \in L} B_{km,f} + \sum_{mn \in L} B_{mn,f} \right) \frac{V_{m,f}^{re}}{2} = I_{m,f}^{Dim} - I_{n,f}^{cbim} \quad \forall n \in N, f \in F \tag{3.130}$$

where $I_{n,f}^{cbre}$ and $I_{n,f}^{cbre}$ are the real and imaginary parts of the current injected in phase f, by the SCB connected and node n.

Power-Based Representation—Capacitor Banks: For this formulation, the Q^{cb} is included in the reactive power balance as shown in (3.131).

$$\sum_{km \in L} Q_{km,f} - \sum_{mn \in L} \left(Q_{mn,f} + Q_{mn,f}^{L} \right) + Q_{m,f}^{G} = Q_{m,f}^{D} - Q_{m}^{cb} \quad \forall m \in N, f \in F \tag{3.131}$$

3.7.2 On-Load Tap Changers and Voltage Regulators

OLTCs and VRs are the devices in charge of controlling the voltage magnitudes in the electric distribution network, within a VVC environment. These devices adjust their input voltage through tap changing, and their operation can be represented under the same mathematical formulation. Thus, let $RT \subseteq L$ be the set of circuits where a VR is installed. $tp_{mn,f}$ is the integer variable that defines the tap position for the VR installed in circuit mn, in phase f; while, $Tp_{mn,f}$ is the maximum number of taps; and $\%R_{mn}$ is the regulation percentage.

Independent of the steady-state formulation adopted, (3.132) represents the minimum and maximum limits of the tap position. Analogue to CB, the number of

tap changes permitted along the entire time period must be limited in a multi-period optimization; hence, under such scenario (3.133) must be taken into account.

$$-Tp_{mn} \leq tp_{mn,f} \leq Tp_{mn} \quad \forall mn \in RT, f \in F \tag{3.132}$$

$$\sum_{t \in T} \left| tp_{mn,f,t} - tp_{mn,f,t-1} \right| \leq \Delta^{vr} \quad \forall mn \in RT, f \in F \tag{3.133}$$

Current-Based Representation—OLTCs and VRs: In this formulation, (3.134) and (3.135) represent the real and imaginary regulated voltage; while, (3.136) and (3.137) represent the real and imaginary regulated current on each VR.

$$V^{re}_{n,f} = (1 + \%R_{mn} tp_{mn,f} / Tp_{mn}) V^{re}_{m,f} \quad \forall mn \in RT, f \in F \tag{3.134}$$

$$V^{im}_{n,f} = (1 + \%R_{mn} tp_{mn,f} / Tp_{mn}) V^{im}_{m,f} \quad \forall mn \in RT, f \in F \tag{3.135}$$

$$I^{re}_{km,f} = (1 + \%R_{mn} tp_{mn,f} / Tp_{mn}) I^{re}_{mn,f} \quad \forall mn \in RT, f \in F \tag{3.136}$$

$$I^{im}_{km,f} = (1 + \%R_{mn} tp_{mn,f} / Tp_{mn}) I^{im}_{mn,f} \quad \forall mn \in RT, f \in F \tag{3.137}$$

Equations (3.134)–(3.137) represent the operation of VRs and OLTCs in terms of the real and imaginary voltages and currents of the electric distribution network. Nevertheless, the nonlinearities presented have to be addressed, i.e., the product of the decision variables $tp_{mn,f}$ and, $V_{m,f}$ or $I_{mn,f}$ on the real and imaginary components. In this regard, the integer number of steps is represented as a set of binary variables $bt_{mn,f}$ and the products $tp_{mn,f} V_{m,f}, tp_{mn,f} I_{mn,f}$ are substituted by auxiliary variables $V^{c}_{mn,f,k}$ and $I^{c}_{mn,f,k}$, respectively.

A linear extension for (3.134)–(3.137) is presented in (3.138)–(3.151), where (3.138) and (3.139) represent the calculation of the regulated voltage, and, (3.140) and (3.141) the calculation of the regulated current. Constraint (3.142) associates the set of binary variables with the tap integer variable. Equations (3.143) and (3.144), and (3.145) and (3.146), define the auxiliary variables $V^{c}_{mn,f,k}$ and $I^{c}_{mn,f,k}$ respectively while (3.147) and (3.148), and (3.149) and (3.150) describe their limits. Finally, (3.151) represents the sequencing of the binary variable $bt_{mn,f}$.

$$V^{re}_{n,f} = (1 - \%R_{mn}) V^{re}_{m,f} + \sum_{k=1}^{2Tp_{mn}} \frac{\%R_{mn}}{Tp_{mn}} V^{c(re)}_{mn,f,k} \quad \forall mn \in RT, f \in F \tag{3.138}$$

$$V^{im}_{n,f} = (1 - \%R_{mn}) V^{im}_{m,f} + \sum_{k=1}^{2Tp_{mn}} \frac{\%R_{mn}}{Tp_{mn}} V^{c(im)}_{mn,f,k} \quad \forall mn \in RT, f \in F \tag{3.139}$$

$$I^{re}_{km,f} = (1 - \%R_{mn})I^{re}_{mn,f} + \sum_{k=1}^{2Tp_{mn}} \frac{\%R_{mn}}{Tp_{mn}} I^{c(re)}_{mn,f,k} \quad \forall mn \in RT, f \in F \tag{3.140}$$

$$I^{im}_{km,f} = (1 - \%R_{mn})I^{im}_{mn,f} + \sum_{k=1}^{2Tp_{mn}} \frac{\%R_{mn}}{Tp_{mn}} I^{c(im)}_{mn,f,k} \quad \forall mn \in RT, f \in F \tag{3.141}$$

$$\sum_{k=1}^{2Tp_{mn}} bt_{mn,f,k} - Tp_{mn} = tp_{mn,f} \quad \forall mn \in RT, f \in F \tag{3.142}$$

$$\left| V^{re}_{m,f} - V^{c(re)}_{mn,f,k} \right| \leq \bar{V}(1 - bt_{mn,f,k}) \quad \forall mn \in RT, f \in F, k = 1 \ldots 2Tp_{mn} \tag{3.143}$$

$$\left| V^{im}_{m,f} - V^{c(im)}_{mn,f,k} \right| \leq \bar{V}(1 - bt_{mn,f,k}) \quad \forall mn \in RT, f \in F, k = 1 \ldots 2Tp_{mn} \tag{3.144}$$

$$\left| V^{c(re)}_{mn,f,k} \right| \leq \bar{V} bt_{mn,f,k} \quad \forall mn \in RT, f \in F, k = 1 \ldots 2Tp_{mn} \tag{3.145}$$

$$\left| V^{c(im)}_{mn,f,k} \right| \leq \bar{V} bt_{mn,f,k} \quad \forall mn \in RT, f \in F, k = 1 \ldots 2Tp_{mn} \tag{3.146}$$

$$\left| I^{re}_{mn,f} - I^{c(re)}_{mn,f,k} \right| \leq \bar{I}_{mn}(1 - bt_{mn,f,k}) \quad \forall mn \in RT, f \in F, k = 1 \ldots 2Tp_{mn} \tag{3.147}$$

$$\left| I^{im}_{mn,f} - I^{c(im)}_{mn,f,k} \right| \leq \bar{I}_{mn}(1 - bt_{mn,f,k}) \quad \forall mn \in RT, f \in F, k = 1 \ldots 2Tp_{mn} \tag{3.148}$$

$$\left| I^{c(re)}_{mn,f,k} \right| \leq \bar{I}_{mn} bt_{mn,f,k} \quad \forall mn \in RT, f \in F, k = 1 \ldots 2Tp_{mn} \tag{3.149}$$

$$\left| I^{c(im)}_{mn,f,k} \right| \leq \bar{I}_{mn} bt_{mn,f,k} \quad \forall mn \in RT, f \in F, k = 1 \ldots 2Tp_{mn} \tag{3.150}$$

$$bt_{mn,f,k} \leq bt_{mn,f,k-1} \quad \forall mn \in RT, f \in F, k = 1 \ldots 2Tp_{mn} \tag{3.151}$$

Power-Based Representation—OLTCs and VRs: For the power-based formulation, $V^{sqr}_{m,f}$ is altered by the square of the regulation ratio, which is expressed in terms of the regulation percentage, the tap integer value, and the maximum tap, as shown in (3.152).

$$V^{sqr}_{n,f} = \left(1 + \%R_{mn} \frac{tp_{mn,f}}{Tp_{mn}}\right)^2 V^{sqr}_{m,f} \quad \forall mn \in RT, f \in F \tag{3.152}$$

In order to cope with the nonlinearities observed in (3.152), $tp^2_{mn,f}$ is represented as a set of binary variables $bt_{mn,f}$, and the product $tp^2_{n,f}V^{sqr}_{m,f}$ is represented using the auxiliary variables $V^c_{mn,f}$, as shown in set (3.153)–(3.157).

$$V^{sqr}_{n,f} = \sum_{k=1}^{2Tp_{mn}} \left[\frac{\%R_{mn}}{Tp_{mn}} \left(\frac{(2k-1)\%R_{mn}}{Tp_{mn}} + 2(1-\%R_{mn}) \right) V^c_{mn,f,k} \right] + V^{sqr}_{m,f}(1-\%R_{mn})^2 \quad \forall mn \in RT, f \in F \tag{3.153}$$

$$\underline{V}^2(1-bt_{mn,f,k}) \leq V^{sqr}_{m,f} - V^c_{mn,f,k} \quad \forall mn \in RT, f \in F, k = 1\ldots 2Tp_{mn} \tag{3.154}$$

$$V^{sqr}_{m,f} - V^c_{mn,f,k} \leq \bar{V}^2(1-bt_{mn,f,k}) \quad \forall mn \in RT, f \in F, k = 1\ldots 2Tp_{mn} \tag{3.155}$$

$$\underline{V}^2 bt_{mn,f,k} \leq V^c_{mn,f,k} \leq \bar{V}^2 bt_{mn,f,k} \quad \forall mn \in RT, f \in F, k = 1\ldots 2Tp_{mn} \tag{3.156}$$

$$bt_{mn,f,k} \leq bt_{mn,f,k-1} \quad \forall mn \in RT, f \in F, k = 2\ldots 2Tp_{mn} \tag{3.157}$$

Therefore, the complete MILP formulations for VVC optimization considering operational limits, are presented in (3.158) and (3.159), for the current-based and power-based representations, respectively.

$$\begin{gathered}\min \alpha \\ \text{subject to} : (3.6)-(3.9), (3.15), (3.16), (3.52), (3.53), (3.57), (3.61)-(3.63), (3.124), (3.125), \\ (3.127)-(3.130), (3.132), \text{and } (3.138)-(3.151)\end{gathered} \tag{3.158}$$

$$\begin{gathered}\min \alpha \\ \text{subject to} : (3.31), (3.41)-(3.43), (3.54), (3.58), (3.61), (3.64), (3.65), (3.124), (3.125), \\ (3.131), (3.132), \text{and } (3.153)-(3.157)\end{gathered} \tag{3.159}$$

3.8 Mathematical Framework Application in Control Approaches

Two control applications are presented in this section to assess the presented mathematical optimization framework. Initially, the EVCC problem is tackled using the current-based formulation, as shown in [25]. Later, a voltage control using the power-based LP formulation is shown, solving a VVC scheme to reduce voltage deviation and guarantee proper operation of the electric distribution network.

3.8.1 Electric Vehicle Charging Coordination Problem

The EV charging coordination problem consists in determining the optimal schedule for charging the EV batteries aiming an economical operation of the electric distribution network, while maintaining a suitable and efficient system operation. Hereby, a multi-period MILP formulation was proposed in [25] to solve the optimal charging coordination of EVs in unbalanced distribution networks considering V2G technology and DG. The steady-state operation of the grid is represented using the current-based formulation. The MILP formulation is embedded in a step-by-step control method that considers randomness in EV arrival, departure, and initial SOC.

The multi-period approach studies a specific time period which is divided into several time intervals. The control method finds an optimal schedule for the energy exchange between EV batteries and the grid. This method solves the proposed MILP model at the beginning of each time interval, constructing a step-by-step solution over the entire time period. The solution presents a charging schedule for each EV, which is generated between arrival and departure, ideally dispatching a fully charged battery.

The objective function of the EVCC problem, presented in (3.160), seeks to minimize the cost of the energy provided by the substation and the DG units as well as to reduce energy curtailment in EVs (if an EV cannot be completely charged, the unserved energy is considered as an energy curtailment).

$$\min \sum_{f\in F}\sum_{t\in T}\alpha_{S,t}^{G}\Delta_t\left(V_{S,f,t}^{re}I_{S,f,t}^{Gre}+V_{S,f,t}^{im}I_{S,f,t}^{Gim}\right)+\sum_{n\in N}\sum_{t\in T}\alpha_{n,t}^{DG}\Delta_t P_{n,t}^{DG}+\sum_{e\in EV}\beta E_e^{SH} \tag{3.160}$$

where $\alpha_{S,t}^{G}$ and $\alpha_{n,t}^{DG}$ are the energy costs at the substation and for each DG unit in time interval t, respectively. E_e^{SH} is the energy curtailment for EV e, while β is the EV curtailment cost (typically a high value to avoid curtailment).

Furthermore, the steady-state operation of the distribution network was modeled using (3.6), (3.7), (3.15), (3.16), (3.161), and (3.162). Constraints (3.52), (3.53), and (3.57), were used represent the operational limits. The DG units were modeled using (3.95), (3.96), (3.97), (3.103), and (3.104); an additional limit for the active power was also employed. Finally, the operation of the EVs was represented by (3.84)-(3.88), and (3.163).

$$\begin{aligned} &I_{m,f}^{Gre}+I_{m,f}^{DGre}+\sum_{km\in L}I_{km,f}^{re}-\sum_{mn\in L}I_{mn}^{re}-\left(\sum_{km\in L}B_{km,f}+\sum_{mn\in L}B_{mn,f}\right)\frac{V_{m,f}^{im}}{2}\\ &\quad=I_{m,f}^{Dre}+\sum_{e\in EV}I_e^{EVre}\gamma_{e,m,f}\\ &\quad\forall m\in N, f\in F \end{aligned} \tag{3.161}$$

$$I_{m,f}^{Gim} + I_{m,f}^{DGim} + \sum_{km \in L} I_{km,f}^{im} - \sum_{mn \in L} I_{mn}^{im} - \left(\sum_{km \in L} B_{km,f} + \sum_{mn \in L} B_{mn,f} \right) \frac{V_{m,f}^{re}}{2} = I_{m,f}^{Dim} + \sum_{e \in EV} I_e^{EVim} \gamma_{e,m,f} \quad \forall m \in N, f \in F \tag{3.162}$$

$$\bar{E}_e^{EV} = E_e^{EVi} + \sum_{t \in T} \Delta t (\bar{P}_e^{EV+} y_{e,t} \eta_e^{EV+} - \bar{P}_e^{EV-} z_{e,t} \eta_e^{EV-}) + E_e^{SH} \quad \forall e \in EV \tag{3.163}$$

The proposed model was tested in the IEEE 123-node test system [11], and the following considerations were taken into account:

- Phases A, B, and C of the electric distribution network were charged with 1.42 MVA (40.7%), 0.915 MVA (26.2%), and 1.155 MVA (33.1%), respectively.
- The time period was set from 18:00 to 08:00 h, divided into half-hour time intervals.
- Two types of EV batteries were considered: 50 kWh Tesla EVs and 20 kWh Nissan Leafs. The charging maximum power was 10 and 4 kW, and for EV-V2Gs the discharging maximum power was 5 and 2 kW, respectively.
- Hourly energy cost and load variation were considered.
- The arrival and departure time intervals were generated based on the two chi-squared probability functions with 8 and 4 degrees of freedom.
- The initial SOC of the EVs was generated using the normal-based probability function with mean value and the standard deviation of 15 and 10, respectively.
- The minimum voltage limit was set at 0.90 pu.
- The maximum current was 500 A for all feeders.
- 400 EVs were plugged into the grid.
- 40% of EVs were considered to have V2G technology.

The model was implemented in the mathematical programming language AMPL [12] and solved with the commercial solver CPLEX [3]. Initially, the dumb charge case is presented. Here, the EV recharge was done without any charging coordination, i.e., the EV batteries started an uninterrupted charging process as soon as they were plugged into the electric distribution network. Later, several control scenarios were analyzed. Figure 3.6 shows the energy exchange between the EVs

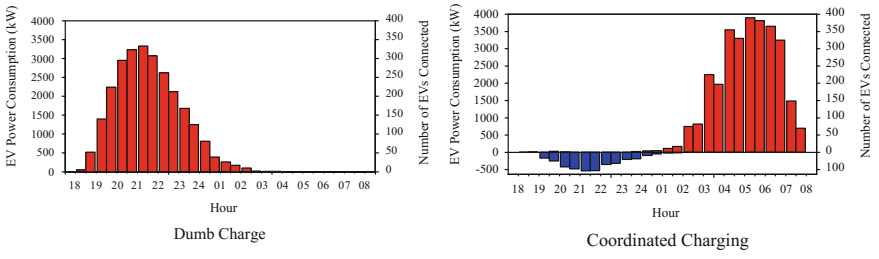

Fig. 3.6 EV active power exchange [25]

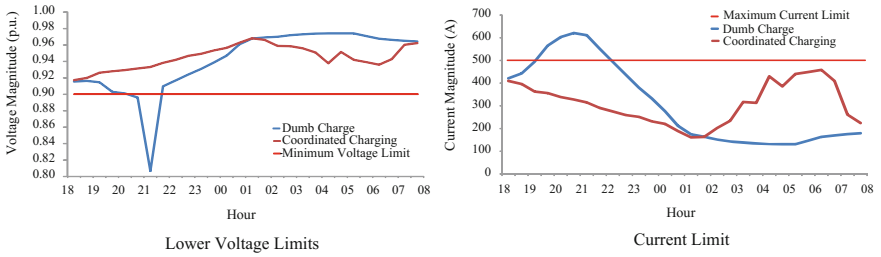

Fig. 3.7 Operational limits [25]

and the grid for the dumb charge and a coordinated charge scenario, in which all EVs were considered 'Tesla EV'. For the coordinated charge case, the objective function was reduced by 25% when compared to the dumb charge case, and no curtailment was presented.

The power related to the charging and discharging of EVs is shown in red and blue, respectively. Following convention, the EV charging power and the EV-V2G discharging power are given in positive and negative values, respectively. It can be seen that without any coordination (Dumb Charge), the EV batteries were continuously charged upon arrival; hence, the peak load for this case was between 21:00 and 22:00. In the coordinated charge case, this peak was shifted to the low-cost time intervals. This represented a reduction of almost 1 MW in the total active power demand.

Figure 3.7 presents the voltage and thermal limits for these cases. For the dumb charge, voltage and current limit violations were presented. These breaches were avoided when the EV charging control was enabled. Hence, it is stated that the EVCC in the distribution network is beneficial not only for peak load reduction, but also for maintaining the proper operation of the grid.

Therefore, the step-by-step methodology based on the current-based MILP formulation was proved efficient to find an optimal charging schedule for EVs in unbalanced network considering V2G technology.

3.8.2 Voltage Control Problem

High voltage drops along a radial distribution feeder lead to elevated energy losses. Hence, control methods for voltage optimization are crucial in daily distribution network operation. The application of the power-based formulation in the voltage control method is evaluated using the IEEE 13-node test system [11].

Figure 3.8 shows the IEEE 13-node test system, which has nominal conventional demand of 1.31 MVA (34.2%), 1.16 MVA (30.3%), and 1.36 MVA (35.5%), connected to phases A, B, and C, respectively. For this test, all loads are considered to be connected in wye-configuration and classified as constant power. Moreover,

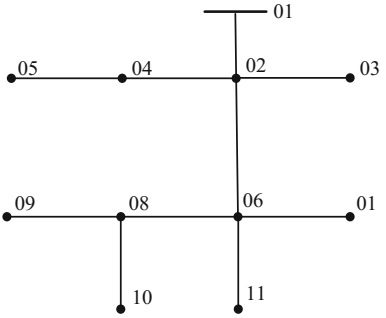

Fig. 3.8 IEEE 13-node test system

Table 3.3 Voltage profile of the IEEE 13-node test system, under nominal demand (pu)

Bus\Phase	A	B	C
1	1.0000	1.0000	1.0000
2	0.9555	0.9695	0.9347
3	0.9523	0.9675	0.9319
4	–	0.9591	0.9378
5	–	0.9557	0.9389
6	0.9221	0.9723	0.8585
7	0.9138	0.9734	0.8545
8	0.9200	–	0.8546
9	–	–	0.8508
10	0.9138	–	–
11	0.9221	0.9723	0.8585

the nominal voltage is 4.16 kV, and the voltage magnitude at the substation is fixed at 1.0 pu. Working under nominal demand, the test system shown in Fig. 3.8, presents the voltage profile shown in Table 3.3.

In order to improve the voltage profile of the electric distribution network, the minimum and maximum voltage limits are set at 0.93 and 1.05 pu, respectively. An OLTC and two switchable SCB are added to the grid in order to fulfill voltage limit requirements. It is desired to use these devices to keep the voltage between the established limits, while minimizing the voltage deviation at each bus for 4 different load levels, 100, 70, 50, and 30% of the nominal demand (i.e., it is expected to maintain the voltage magnitude of all buses as close as possible to the nominal value).

Hence, the control actions for each device should be determined in order to fulfill the operational constraints related to the voltage limit, while minimizing voltage deviation. In this matter, consider:

- The OLTC is installed at the substation and controls the voltage magnitude at node 1.
- The OLTC can vary the input voltage magnitude in a 5% regulation ratio, distributed in 8 tap positions (±4).

- The switchable SCBs are installed at node 7 and 9.
- Each switchable SCB has 6 × 500 kvar, modules.

To determine the control actions for the OLTC and the BCs, the power-based LP formulation is chosen. Initially the voltage deviation (ψ) is expressed as the absolute value of the difference between nominal voltage $\left(V_{nom}^2\right)$ and the square value of the bus voltage $\left(V_{n,f}^{sqr}\right)$, as shown in (3.164). Thus, (3.164) is linearized in (3.165) and (3.166) taking advantage that the deviation is minimized in the objective function.

$$\left|V_{nom}^2 - V_{n,f}^{sqr}\right| = \psi_{n,f} \quad \forall n \in N, f \in F \tag{3.164}$$

$$V_{nom}^2 - V_{n,f}^{sqr} \leq \psi_{n,f} \quad \forall n \in N, f \in F \tag{3.165}$$

$$-\left(V_{nom}^2 - V_{n,f}^{sqr}\right) \leq \psi_{n,f} \quad \forall n \in N, f \in F \tag{3.166}$$

The LP formulation presented in Sect. 3.7 is used, and the complete MILP is shown as

$$\begin{gathered}\min \sum_{n \in N} \sum_{f \in F} \psi_{n,f} \\ \text{subject to} : (3.31), (3.41) - (3.43), (3.54), (3.58), (3.61), (3.64), (3.65), (3.124), (3.125), \\ (3.131), (3.132), (3.153) - (3.157), (3.165), \text{and } (3.166)\end{gathered} \tag{3.167}$$

The mathematical formulation was written in the mathematical language AMPL [12], and solved using CPLEX [3]. The model was solved for the four load levels, finding the best configuration for each case. Table 3.4 presents for each case the tap position for the OLTC, the number of enabled modules for the SCBs, and the total deviation. Besides, it can be seen that the voltage limits were fulfilled for each case in which the devices were taken into account.

Table 3.4 Summary of the results for the Voltage Control Problem

Case	Loading (%)	OLTC-Tap	SCB-7 modules active/ total	SCB-9 modules active/ total	Voltage deviation (pu)	Voltage limits
w/o devices	100	–	–	–	4.0177	Breached
I	100	+3	6/6	6/6	1.2943	Fulfilled
II	70	+2	6/6	6/6	0.7122	Fulfilled
III	50	+1	6/6	5/6	0.4937	Fulfilled
IV	30	+1	1/6	3/6	0.2783	Fulfilled

Table 3.5 Voltage profile of the IEEE 13-node test system, after voltage control implementation (pu)

Phase	A		B		C	
Bus\Case	w/o devices	I	w/o devices	I	w/o devices	I
1	1.0000	1.0375	1.0000	1.0375	1.0000	1.0375
2	0.9555	0.9980	0.9695	1.0067	0.9347	1.0017
3	0.9523	0.9949	0.9675	1.0048	0.9319	0.9991
4	–	–	0.9591	0.9967	0.9378	1.0046
5	–	–	0.9557	0.9934	0.9389	1.0056
6	0.9221	0.9693	0.9723	1.0076	0.8585	0.9594
7	0.9138	0.9622	0.9734	1.0092	0.8545	0.9566
8	0.9200	0.9672	–	–	0.8546	0.9601
9	–	–	–	–	0.8508	0.9608
10	0.9138	0.9613	–	–	–	–
11	0.9221	0.9693	0.9723	1.0076	0.8585	0.9594

To better illustrate the solution found through mathematical optimization, the voltage profile for the solution determined by the MILP formulation under nominal demand, is shown in Table 3.5. It can be seen that the MILP formulation found a solution which guarantee the compliance of the voltage limits.

Voltage limit violations were highlighted in red. The efficiency of the power-based MILP formulation was proven as the solutions for all cases improved the voltage profile, keeping all voltage magnitudes in between the limits, while minimizing the voltage deviation.

3.9 Comparative Overview and Discussion

The formulations presented, efficiently model the steady-state operation of unbalanced networks; constituting a mathematical framework that can be used by planners and operators as a tool inside optimization methods and algorithms, aiming to optimize specific goals. Although both formulations target the same objective, the planner/operator can choose the one that better accommodates and fits the problem that he is aiming to tackle. In order to make this decision, the following considerations must be addressed and well-thought:

1. Although both formulations show high accuracy determining the steady-state operation point, the current-based model slightly outperforms the power-based, as shown in Sect. 3.2.3.

2. Due to its representation in terms of the real and imaginary parts of voltages and currents, modeling operational limits within the current-based formulation requires a high number of constraints. This fact conveys to higher computational burden, which can slow down the solution process especially in large-scale test systems.
3. In optimization methods or algorithms applied over non-stressed test systems, where operational limits are not a concern to the optimizer (e.g., demand response or market-based optimizations), the current-based formulation may highlight as a better option.
4. As mentioned, both formulations can handle optimizations algorithms taking into account smart grid devices plugged into the network. Nevertheless, the mathematical representation of the considered smart grid devices can sway the formulation choice; e.g., in a volt-var approach, the power-based formulation is recommended, as the volt-var devices influence directly over the voltage magnitude and reactive power flows.
5. Finally, the load behavior is also an important feature to take into account as it impacts directly in the operation point estimation. Both LP formulations rely on the accuracy of the estimated operation point. In this regard, in little observable distribution networks, estimating voltages is an easier task to the planner/operator than estimating power flows along the grid. Hence, the current-based formulation will suit better to this application.

It is important to remark that every optimization problem targeted in electric distribution network will bring specific considerations that have to be analyzed to make the best choice.

Appendix 1: Piecewise Linearization Technique

The piecewise linearization is a technique in which a nonlinear function is approximated using a set of piecewise linear functions [37]. Widely used in engineering, this technique is often employed to cope with quadratic nonlinearities, helping to reach LP models. Typically, a function f is defined in order to calculate the square value of a variable σ, represented as $\sigma^+ + \sigma^-$ and limited by the interval $[0, \bar{\sigma}]$. This type of function has a general structure, as

$$f(\sigma, \bar{\sigma}, \Lambda) = \sum_{\lambda=1}^{\Lambda} \phi_{\sigma,\lambda} \Delta_{\sigma,\lambda} \tag{3.168}$$

$$\sigma = \sigma^+ - \sigma^- \tag{3.169}$$

$$\sigma^{+} + \sigma^{-} = \sum_{\lambda=1}^{\Lambda} \Delta_{\sigma,\lambda} \tag{3.170}$$

$$0 \leq \Delta_{\sigma,\lambda} \leq \bar{\sigma}/\Lambda \quad \forall \lambda \in \Lambda \tag{3.171}$$

$$\phi_{\sigma,\lambda} = (2\lambda - 1)\bar{\sigma}/\Lambda \quad \forall \lambda \in \Lambda \tag{3.172}$$

The parameter $\phi_{\sigma,\lambda}$ is calculated to compute the contribution of $\Delta_{\sigma,\lambda}$ in each step of the discretization. The parameter $\bar{\sigma}$ represents the maximum value of σ, while Λ is the number of discretizations used in the linearization.

It is important to remark that this approach is limited to maximizing strictly concave functions or minimizing convex functions. If the application of this technique under different conditions is desired, the inclusion of binary variables and additional constraints is mandatory.

Appendix 2: Multi-period and Multi-scenario Extension

Typically, optimization analyses in electric distribution network operation are done along a time window in which several control actions have be defined and they may be dependent among them; this is known as multi-period optimization. For example, the day-ahead operation planning is typically divided in one-hour time windows, and the decisions from one hour may or may not affect the decisions regarding the next time intervals. Thus, mathematical formulations for the distribution network operation should be able to handle multi-period optimization analyses. In this regard, the LP formulations presented can be easily adapted to handle several time intervals. Hence, a new index associated to the time interval is added to the variables that represent the distribution network operation (e.g., voltages, currents, and power flows).

Furthermore, adaptability to multi-scenario optimizations is also required in an optimization framework for electric distribution network to model the uncertainty in the grid. The multi-scenario optimization is a method usually employed to solve stochastic programming problems in which some of the variables or parameters are of uncertain nature (e.g., EV behavior, renewable DG availability, and demand variations). The uncertainties are represented through a set of scenarios and each one with an associated probability, i.e., a multi-scenario model will provide an optimal solution on average, considering all the scenarios simultaneously. Analogue to the multi-period case, a new index is added to the uncertain variables associated to each scenario. Thereby, the objective function of the problem is calculated as the expected value due to the inclusion of the probabilities related to each scenario.

Appendix 3: Estimated Steady-State Operation Point

As mentioned in Sect. 3.2.3, the accuracy of the presented three-phase formulations relies on the precision of the estimated operation point. High quality estimations will minimize the error corresponding to some approximations in voltage magnitudes and some linearization techniques (e.g., Taylor's linearization). In order to obtain a suitable estimated operation point, the followings techniques might be employed:

1. A two-stage approach, in which a first stage solves the LP model using a flat start (e.g., assuming nominal voltages and disregarding power). Later, the solution of the first stage is used to initialize the second stage in which the LP model is once again solved from the already calculated operating point.
2. Using historical data, where historical data is used in order to determine the estimated values. Typically, the operator's knowledge and experience are crucial to select previous operating points which have occurred under similar loading and generation scenarios.
3. Using the previous time interval operating point is another technique for the estimation of the operating point. This approach is commonly used on small time interval optimization approaches in which abrupt changes in the demand are not expected (e.g., EVCC problems).

It is important to remark that the estimation of the operation point is an important issue to be taken into account when applying the presented formulations. Furthermore, the technique chosen to determine the estimated operation point will depend on the information available and the characteristics of the problem that is being tackled.

References

1. J.A. Momoh., *Electric Power System Applications of Optimization*, 2nd edn. (CRC Press, Boca Raton, 2009)
2. L. Aleixo et al., A general framework for active distribution network planning, in *CIGRE Symposium 2013*, no. April 2013 (2013), pp. 1–8
3. "IBM ILOG CPLEX V12.1 User's Manual for CPLEX." CPLEX Division, Incline Village, NV (2009)
4. MOSEK ApS, *The MOSEK optimization tools manual—version 6.0*. Copenhagen, 2009
5. G. O. Inc., Gurobi Optimizer reference manual, www.Gurobi.com, vol. 6 (2014), p. 572
6. R.H. Byrd, J. Nocedal, R.A. Waltz, Knitro: an integrated package for nonlinear optimization, in *Large–Scale Nonlinear Optimization*, ed. by G. Di Pillo, M. Roma (Springer US, Boston, MA, 2006), pp. 35–59
7. P. Bonami, J. Lee, BONMIN Users' Manual, (2007)
8. D. Shirmohammadi, H.W. Hong, A. Semlyen, G.X. Luo, A compensation-based power flow method for weakly meshed distribution and transmission networks. IEEE Trans. Power Syst. **3**(2), 753–762 (1988)

9. R.G. Cespedes, New method for the analysis of distribution networks. IEEE Trans. Power Deliver. **5**(1), 391–396 (1990)
10. J.F. Franco, M.J. Rider, R. Romero, A mixed-integer linear programming model for the electric vehicle charging coordination problem in unbalanced electrical distribution systems. IEEE Trans. Smart Grid **6**(5), 2200–2210 (2015)
11. IEEE/PES, Distribution Test Feeders, 123-bus Feeder.
12. R. Fourer, D.M. Gay, B.W. Kernighan, *AMPL: a modeling language for mathematical programming*, 2nd edn. (Brooks/Cole-Thomson Learning, Pacific Grove, CA, 2003)
13. EPRI, Open Distribution System Simulator, (2012)
14. International energy outlook 2013. (2013)
15. P.L. Dandeno et al., System load dynamics-simulation effects and determination of load constants. IEEE Trans. Power Appar. Syst. **PAS-92** (1973)
16. A. Padilha-Feltrin, D. Quijano, J.R. Mantovani, Volt-VAR multiobjective optimization to peak-load relief and energy efficiency in distribution networks. IEEE Trans. Power Deliver. **30**(2), 618–626 (2015)
17. H. Ahmadi, J.R. Martí, H.W. Dommel, A framework for volt-VAR optimization in distribution systems. IEEE Trans. Smart Grid **6**(3), 1473–1483 (2015)
18. C. Sabillon, O. Melgar Dominguez, J. Franco, M. Lavorato, M.J. Rider, Volt-VAR control and energy storage device operation to improve the electric vehicle charging coordination in unbalanced distribution networks. IEEE Trans. Sustain. Energy (2017)
19. L.M. Korunovic, S. Sterpu, S. Djokic, K. Yamashita, S. M. Villanueva, J.V. Milanovic, Processing of load parameters based on Existing Load Models, in *2012 3rd IEEE PES Innovative Smart Grid Technologies Europe (ISGT Europe)* (2012), pp. 1–6
20. Task force on load representation for dynamic performance IEEE, Bibliography on load models for power flow and dynamic performance simulation. IEEE Trans. Power Syst. **10** (1), 523–538 (1995)
21. N. Anglani, F. Fattori, G. Muliere, Electric vehicles penetration and grid impact for local energy models, in *2012 IEEE International Energy Conference and Exhibition (ENERGYCON)* (2012), pp. 1009–1014
22. K. Clement-Nyns, E. Haesen, J. Driesen, The impact of charging plug-in hybrid electric vehicles on a residential distribution grid. IEEE Trans. Power Syst. **25**(1), 371–380 (2010)
23. D. Wu, D.C. Aliprantis, K. Gkritza, Electric energy and power consumption by light-duty plug-in electric vehicles. IEEE Trans. Power Syst. **26**(2), 738–746 (2011)
24. A. O'Connell, A. Keane, D. Flynn, Rolling multi-period optimization to control electric vehicle charging in distribution networks, in *2014 IEEE PES General Meeting|Conference Exposition* (2014), p. 1
25. C. Sabillon Antunez, J.F. Franco, M.J. Rider, R. Romero, A new methodology for the optimal charging coordination of electric vehicles considering vehicle-to-grid technology. IEEE Trans. Sustain. Energy **7**(2), 596–607 (2016)
26. A.T. Al-Awami, E. Sortomme, Coordinating vehicle-to-grid services with energy trading. IEEE Trans. Smart Grid **3**(1), 453–462 (2012)
27. T. Ackermann, G. Andersson, L. Söder, Distributed generation: a definition. Electr. Power Syst. Res. **57**(3), 195–204 (2001)
28. K. Qian, C. Zhou, Y. Yuan, X. Shi, M. Allan, Analysis of the environmental benefits of Distributed Generation, in *IEEE Power and Energy Society 2008 General Meeting: Conversion and Delivery of Electrical Energy in the 21st Century, PES* (2008)
29. A.C. Rueda-Medina, J.F. Franco, M.J. Rider, A. Padilha-Feltrin, R. Romero, A mixed-integer linear programming approach for optimal type, size and allocation of distributed generation in radial distribution systems. Electr. Power Syst. Res. **97**, 133–143 (2013)
30. J.A.P. Lopes, N. Hatziargyriou, J. Mutale, P. Djapic, N. Jenkins, Integrating distributed generation into electric power systems: a review of drivers, challenges and opportunities. Electr. Power Syst. Res. **77**(9), 1189–1203 (2007)
31. M. Bollen, F. Hassan, *Integration of Distributed Generation in the Power System* (2011)

32. Y.M. Atwa, E.F. El-Saadany, MMa. Salama, R. Seethapathy, Optimal renewable resources mix for distribution system energy loss minimization. IEEE Trans. Power Syst. **25**(1), 360–370 (2010)
33. S. Weckx, C. Gonzalez, J. Driesen, Combined central and local active and reactive power control of PV inverters. IEEE Trans. Sustain. Energy **5**(3), 776–784 (2014)
34. R. Tonkoski, L.A.C. Lopes, T.H.M. El-Fouly, Coordinated active power curtailment of grid connected PV inverters for overvoltage prevention. IEEE Trans. Sustain. Energy **2**(2), 139–147 (2011)
35. M. Ross, R. Hidalgo, C. Abbey, G. Joos, Analysis of energy storage sizing and technologies, in *EPEC 2010—IEEE Electrical Power and Energy Conference: "Sustainable Energy for an Intelligent Grid"* (2010)
36. M.S. ElNozahy, T.K. Abdel-Galil, M.M.A. Salama, Probabilistic ESS sizing and scheduling for improved integration of PHEVs and PV systems in residential distribution systems. Electr. Power Syst. Res. **125**, 55–66 (2015)
37. J.F. Franco, M.J. Rider, M. Lavorato, R. Romero, A mixed-integer LP model for the reconfiguration of radial electric distribution systems considering distributed generation. Electr. Power Syst. Res. **97**, 51–60 (2013)